Baristeas, N., Anka, Z., di Primio, R., Rodriguez, J.F., Marchal, D., Dominguez, F. (2012): Distribution of hydrocarbon leakage indicators in the Malvinas Basin, offshore Argentine continental margin. - Marine Geology, 332-334, 56-74

DOI: 10.1016/j.margeo.2012.09.011

Distribution of hydrocarbon leakage indicators in the Malvinas Basin, offshore Argentine continental margin

N. Baristeas[(1)*]; Z. Anka[(1)]; R. di Primio[(1)]; J. F. Rodriguez[(2)]; D. Marchal[(2)], F. Dominguez[(2)]

(1) Helmholtz-Centre Potsdam - GFZ German Research Centre for Geosciences, Potsdam, Germany.

(2) Petrobras Argentina Energía S.A., Buenos Aires, Argentina.

[*] Corresponding author: baristeas@gfz-potsdam.de

Abstract:

The Malvinas Basin is located in the southernmost Argentinian continental margin. Despite the lack of commercial hydrocarbon accumulation discoveries, the presence of thermogenic gas in gravity cores and seafloor oil slicks point to the existence of an active petroleum system in this basin.

Based on the analysis of over 1000 2D industrial seismic-reflection profiles, covering the shelf and upper-slope of the Malvinas Basin offshore the southernmost Argentinian margin, we document the presence of buried and present-day features including subsurface seismic chimneys, seabed and buried pockmarks, and buried-mounded structures which are probably indicators of long-term leakage history of both liquid and gaseous hydrocarbons since the Eocene to the Present.

Based on their distribution and likely controlling factors, these leakage features were classified into four areas of leakage: Area I to area IV. Area I is located in the centre of the basin and contains seismic anomalies as pipes originating above or in a polygonal faulted Pliocene-Miocene interval accompanied by bright spots and seabed pockmarks. Area IIa/b is located in the south of the basin and contains pipes and buried pockmarks located close to the southern transpressional deformation front. Area III is located to the east of the basin and consists of pipes hosted in a Mid-Cretaceous deltaic-fan. Area IV, located in the western part

of the basin, consists of buried Eocene mounded structures located near the Rio Chico High and above basement highs and faults. They are interpreted as authigenic carbonate mounds possibly derived from oxidation of thermogenic methane that leaked upwards along basement-rooted faults. A reversed-polarity seismic reflection showing a lineation of bright spots has been identified at an average depth of 170 m below seafloor in water depths of about 500 m. We interpret this reflection as a bottom simulating reflector (BSR), which enables us to estimate a geothermal gradient of 23.9 ± 2.0 °C/km for the area. Near and above the thrust faults of a transpressional deformation front, the vertical pipes in area II cross-cut possible hydrate deposits, suggesting that there is a current breaching of these deposits due to tectonically-driven upward focused fluid flow and heat transport.

The gas source for the features observed in areas I, IIa/b and IV is most likely leakage from the uppermost Jurassic-Barremian reservoir Springhill Fm., although a biogenic gas source for leakage indicators in area I can not be ruled out. The leakage indicators in area III are possibly sourced from the Mid-Cretaceous sediments of the Middle Inoceramus Fm.

1. Introduction

In the Malvinas Basin, the existence of an active petroleum system has been proposed in the past (Galeazzi, 1996, and 1998) and the basin has been the target of several seismic reflection and exploratory drilling campaigns since the 70's. Until now, five wells found non-commercial hydrocarbon shows and only one gas chimney has been reported in this basin, identified by the observation of a diffuse, vertical cone-shaped area in 2D seismic reflection data (Richards et al., 2006). In contrast, within the neighbouring Austral-Magallanes Basin, Thomas (1949) reported the occurrence of numerous gas seeps and one oil seep. Since then, several new on- and offshore hydrocarbon discoveries have been made and nowadays the Austral-Magallanes Basin is a productive and proven basin for oil and gas.

Thus, it is interesting that neither commercial oil accumulations nor more evidence of natural gas and oil seeps have been found in the Malvinas Basin, considering that it has a similar geological history to the Austral-Magallanes Basin. In this study we have investigated the possible existence of further evidence of hydrocarbon leakage indicators in the Malvinas Basin and their possible relationship to the evolution of the basin. This contribution aims at improving our understanding of the factors controlling hydrocarbon migration pathways and natural gas leakage in complex tectonic settings offshore South American continental margins.

Seismic manifestations of gas and fluid leakage in marine sediments

One of the most common features observed in marine seismic data associated with recent gas or fluid leakage are vertically elongated zones with a deteriorated seismic signal, which are referred to as pipes or gas chimneys (Cartwright et al., 2007; Judd and Hovland, 2007; Løseth et al., 2009). The form of these zones can range from diffuse broad shadows to sharp well-defined pipe like structures, and from cone- or funnel-shaped features to cigar-shaped features (Løseth et al., 2009).

In this study we use the term "pipe" for features with as straight or cylindrical, elongated vertical shape with a straight to steeply-dipping conical zone that can narrow upwards or downwards (after Cartwright et al., 2007; Moss and Cartwright, 2009; Løseth et al., 2011). The terms "gas chimney" or "seismic chimney" are used in this study in a broader sense for any kind of vertically-elongated features associated with focused fluid flow and gas leakage (after Judd and Hovland, 2007). Pipes are probably linked with very rapid, focused fluid flow as blow out events (Cartwright et al., 2007). They provide a highly-permeable vertical zone along which gas and fluids can migrate very rapidly upwards (Løseth et al., 2009). Focused fluid flow is usually associated with fracture flow out of an overpressured buried reservoir (Løseth et al., 2009), which can be filled with biogenic gases, thermogenic gases, oil, water,

or some combination of these fluids (Gay et al., 2006). In fracture flow, the sealing cap-rock of the overpressured reservoir fails as structural conduits form and dilate, allowing fluids to migrate upwards. These conduits can come from various geological structures, including normal and thrust faults, polygonal faults and hydro-fractures (e.g. Gay et al., 2004; Løseth et al., 2009; Cartwright et al., 2007; Micallef et al., 2011). Polygonal faults provide good leakage pathways. After their generation, deeper fluids can migrate upwards along conduits generated by the intersection of the polygonal faults (Gay et al., 2004). Fluid flow above the intersection of polygonal faults become more focused and can be associated with overlying pipes and pockmarks (Berndt et al., 2003; Cartwright et al., 2007; Gay et al., 2004).

Areas with observed high-amplitude reflection anomalies located above a polygonal faulted interval can indicate the presence of trapped fluids. In these areas, however, often no fluid flow indicators are visible. This could be interpreted as a diffusive fluid flow out of the polygonal faults. Dissolved gas would only result in an amplitude anomaly when it exsolves from the water phase upon pressure decrease during vertical migration. A seismically observable feature, however, would only be developed when a significant amount of gas is trapped under a less permeable layer (Berndt et al., 2003). In this case pipes can be generated when the trap fails, because of exceeding pore pressure of the accumulating gas and fluids (Berndt et al., 2003). This will generate pipes without a clear root point in the underlying polygonal faulted interval.

Free gas accumulations within marine sediment can cause high amplitude reflection anomalies (e.g. bright spots or flat spots) as well as acoustic blanking or turbidity of the seismic signal (Judd and Hovland 2007; Løseth et al., 2009; Gay et al., 2007). These features often occur in the vicinity (on the flanks or directly above) of pipes and gas chimneys (Løseth et al., 2009). Bright spots occur because of the presence of gas within a layer, which reduces the seismic velocity of that layer, thereby increasing the impedance contrast with the neighboring layer. Sometimes a phase reversal between the bright spot and the adjacent layers

is observable (Løseth et al., 2009). Flat spots indicate the gas-water interface between water saturated sediments overlying gas saturated sediments (Judd and Hovland, 2007). Acoustic blanking and turbidity is usually caused by absorption and scattering of acoustic energy of gas charged sediments above the blanking area (Schroot et al., 2005; Gay et al., 2007). Seismic reflections within or adjacent to a gas chimney can be pulled-down or pushed up due to seismic velocity effects, creating v-shaped depressions or a mound-shaped layering (Cartwright et al., 2007; Løseth et al., 2009). The presence of gas, which reduces the velocity, can cause a velocity pull down. Conversely, an increase in sediment velocity, from cementation with authigenic carbonates for example, can cause a velocity pull up.

Pockmarks are common expressions of leakage observed in marine seismic data (Hovland and Judd, 1988; Hovland et al., 2002). These features are cylindrical to elliptical seabed depressions, often seen in 2-D seismic cross-sections as v-shaped depressions. They are associated with gas and/or fluid leakage out of the subsurface and range in depth from meters to tens of meters and in diameter from meters to hundreds of meters (Hovland and Judd, 1988; Judd and Hovland, 2007). They are found on the seafloor and/or as paleo pockmarks on the paleo seabed buried below sediments. Recent pockmarks are often linked with underlying pipes (e.g. Cartwright et al., 2007). Pockmarks are generated by blow outs of fluids (often gas) from the subsurface into the water column, whereby sediment is mobilized and eroded (Judd and Hovland 2007; Løseth et al., 2009). Single v-shaped depressions can be interpreted as pockmarks, whereas stacked v-shaped depressions are more likely generated by velocity pull down effects caused by gas accumulations.

Aside from the above described manifestations of gas in sediments gas leakage is also often associated with gas hydrates and the observation of a bottom simulating reflector (BSR) (e.g. Lüdmann and Wong, 2003; Cathles et al., 2010). Gas hydrates are crystalline, ice like compounds, where gas molecules are trapped within a cage-like structure of the water molecules. They are only stable under specific conditions of depth, temperature, salinity and

water-gas compositions (Sloan, 1990), i.e. in the gas hydrate stability zone (GHSZ). A BSR is the seismic reflection marking the base of the gas hydrate stability zone (BGHSZ), where sediments partially saturated with gas hydrates overlie sediments devoid of hydrate and usually containing free gas (e.g. Bangs et al., 1993). The impedance contrast is negative and a phase reversal is visible compared to the seafloor reflector. In general the BSR follows the seafloor morphology, because the BGHSZ is defined to be the lower stability boundary of gas hydrates, i.e. it follows an isotherm line which is mostly parallel or sub-parallel to the seafloor morphology (Hyndman and Davis, 1992; Hyndman and Spence, 1992).

Another manifestation of fluid and hydrocarbon leakage are mounded structures, associated with hard carbonate formations derived by the microbiological oxidation of leaking methane and further chemosynthetic reactions (Hovland, 1990b). The formation of these so called methane or hydrocarbon derived authigenic carbonates (MDACs or HDACs) (Lein et al., 2004; León et al., 2007) can only occur if methane or hydrocarbons from the subsurface reach the seafloor sediments. Once MDACs or HDACs are generated and the sediment is cemented, organisms can colonize these authigenic carbonate grounds and carbonate mound growth can take place (Judd and Hovland, 2007 and references therein). The process of carbonate mound generation associated with fluid and hydrocarbon leakage is not yet completely understood, but has been observed in several different locations on passive margins around the world. Examples of giant carbonate mounds of deepwater coral reefs at high latitudes are in the Southern Vøring Plateau, offshore Norway (Ivanov et al., 2010) or in the Porcupine Basin, offshore Ireland (Naeth et al., 2005). MDAC and HDAC cemented sediments and dolomite crusts associated with mud mounds have formed in the Gulf of Cadiz (León et al., 2007; Magalhães et al., 2012). Beneath carbonate cemented sediments and mounds, amplitude suppressions is often observed because of the high impedance of the well-indurated structures, which can significantly reduce the transition of energy (Cowley and O'Brien, 2000).

2. General geological background

The study area is within the Malvinas Basin, located on the Argentinean continental shelf offshore the south-easternmost margin of South America, in water depths of about 100 to 600 m (Fig. 1). The basin is bounded by the Malvinas/Falkland Islands to the East and by the Rio Chico High (Dungeness Arch) to the West (Fig. 1). The basin is connected with the Austral-Magallanes Basin to the SW and with the South Malvinas Basin to the SE along a deep basement trough, which is located north of a southern major sinistral transpressional deformation front (Fig. 1). This major transform fault represents the boundary between the South American and Scotia Plates (Ghiglione et al., 2010; Diraison et al., 2000).

The basin infill is influenced by multiple tectonic phases, which develop major stratigraphic unconformities (Biddle et al., 1986; Yrigoyen, 1989; Galeazzi, 1998; Tassone et al., 2008; Ghiglione et al., 2010), (Fig. 2). According to these unconformities, five major tectonic phases have been defined (Yrigoyen, 1989; Galeazzi, 1998), (Fig. 2): 1) the pre-rift phase (168 Ma), 2) the extensional syn-rift phase (168-150.5 Ma), dominated by tuffs, tuffaceous sandstones and rhyolithes, 3) the tectonic sag phase (150.5-68 Ma), which is made up of basal sandstones followed by deep marine fine grained sediments, as shales, silt- and claystones and terminates in a succession of glauconitic sandstones, 4) the extensional foredeep transition phase (68-42.5 Ma), with the development of a deep trough in the south and a reduced sedimentation consisting of a mixture of glauconitic sandstones, claystones, calcareous claystones and carbonates, and 5) the transpressional foredeep phase (42.5 Ma-recent), with the development of the southern transpressional deformation front and increased sedimentation consisting mainly of glauconitic sandstones as well as finer intervals like claystoens and limestones. For more detailed descriptions on the general Geology of the

178 Malvinas Basin, the reader is referred to the works of e.g. Yrigoyen (1989), Galeazzi, (1998),
179 Tassone et al. (2008), and Ghiglione et al. (2010).
180
181 **Petroleum system elements**
182 The petroleum system in the Malvinas Basin is proposed as Lower Inoceramus-Springhill
183 petroleum system (Rossello et al., 2008, and references therein), (Fig. 2). The source rock of
184 this system is the organic rich shale of the Hauterivian-Aptian Lower Inoceramus Fm. (Pampa
185 Rincon Fm.), (Fig. 2), (Biddle et al., 1986; Galeazzi et al., 1998; Rossello et al., 2008).
186 However, a minor source rock interval could also be the Albian-Cenomanian Margas Verdes
187 Fm. (Galeazzi, 1998). Some authors also propose the lacustrine shales of the Jurassic syn-rift
188 Tobífera Fm. and the continental shales of the latest Jurassic-Barremian Springhill Fm. as
189 possible source rocks for the Austral-Magallanes Basin (Pittion and Gouadain, 1992; Bravo
190 and Herrero, 1997; Pittion and Arbe, 1999).
191 Aside fom the fluvial and shoreline sandstones of the Springhill Fm., other minor reservoirs
192 are represented by the Maastrichtian-Eocene glauconitic sandstones or carbonate
193 sediments/mounds and Miocene turbiditic sandstones lobes (Galeazzi, 1998; Rossello et al.,
194 2008).
195 The critical stage of this petroleum system seems to have occured during the Eocene, at the
196 end of the transitional foredeep phase, when the basin had deepened towards the south and the
197 source rock entered into the oil and gas window (Galeazzi, 1998; Ghiglione et al., 2010).
198

199 3. Dataset and Methodology

200 *3.1 Dataset*

201 Over 1000 2D-seismic profiles with a total length of over 65,000 km and a coverage area of
202 over 120,000 km^2 where analysed in this study. The seismic lines were kindly provided by

Petrobras Argentina S.A. in the form of standard industrial reflection lines. They cover a dense grid over the southern Argentinian continental shelf with a grid spacing varying between 2-5 km up to 25-50 km (Fig. 3). The highest grid density is along the western flank of the Rio Chico High and towards the southwest of the basin. The grid density decreases towards the edges of the coverage area. The seismic record depth ranges from 4 to 8 s two-way travel time (twt). The acquisition years of these surveys range from 1970 to 1998. Acquisition information or detailed processing information was not available. Seismic sections from surveys acquired pre-1990 have been scanned and transformed into SEGY standard format. The average frequency range of the seismic signal for all surveys is in a range of about 10-50 Hz, with a dominant frequency at about 20-25 Hz.

The best-quality data come from the 1998 surveys located in the centre of the basin at the eastern part of the coverage area. Despite the limitations due to the low quality of the older data, the 2D seismic grid covers almost the entire basin and provides a very good overview of the basin structure, and allows the detection of hydrocarbon leakage indicators basin-wide. Additionally, Petrobras Argentina S.A. provided information from 25 wells which was used to tie the seismic data with the stratigraphy. Checkshot information from these wells was used for the time-depth conversion of interpreted seismic horizons.

3.2 Methodology

In this study, a detailed seismo-stratigraphic interpretation and mapping of the main unconformities and seismic units in the Malvinas Basin was achieved. The seismic interpretation was carried out using the commercial software Petrel™ (Version 2009.1.1) of Schlumberger. We identified and mapped possible indicators of recent and paleo- gas leakage and the presence of free gas accumulations basin-wide. These indicators include features such as pockmarks, seismic chimneys or pipes, mounded structures, and high amplitude reflection anomalies (e.g. bright spots). In order to determine which of the geological factors control the

hydrocarbon leakage, a detailed correlation between the regional tectonics and the stratigraphy of the basin was carried out.

Local geothermal gradient estimations can be made by using the depth of the observed BSR, if present. The geothermal gradient (g) is thus obtained from:

$$g = (T_{BSR} - T_{ob})/Z_{BSR} \quad (1)$$

where T_{BSR} is the temperature at the BSR depth, T_{ob} is the temperature at the ocean bottom, and Z_{BSR} is the depth of the BSR below the seafloor.

T_{ob} was obtained from the NOAA online database for ocean water temperatures (Locarnini et al., 2010). Several ocean water temperatures, in water depth of 500 m, located above the area of observed BSR, and close to the seafloor (within tens of meters to it), were used to interpolate the temperature on the ocean bottom (Appendix A). T_{BSR} was estimated by Miles' (1995) equations, which are based on the fourth order polynomial fit to the experimental P-T phase boundary curve of methane hydrate in a simplified pure methane-seawater system (Sloan, 1990). In order to convert the BSR depth (Z_{BSR}) from twt into meters, we used a mean sediment velocity of 1700 m/s obtained from a velocity model, which was derived from well checkshot data. For the calculations we estimated an error of ± 0.2°C for the ocean bottom temperature and deviation of ± 50 m/s for the sediment velocity used in the time-depth conversion.

4. Identification of hydrocarbon leakage indicators

In our study area a large number of seismic features were observed, which could be interpreted as possible indications of either paleo- or presently active gas leakage, or as the presence of free gas and gas hydrate deposits in the basin. These features include several vertically-elongated low-amplitude zones, diapir-like structures, high-amplitude anomalies, v-shaped depressions on the seafloor and in the sediments, buried mounded structures, and near-seafloor reflections that we interpret as BSRs.

Figure 4 presents the distribution of the most prominent vertically-elongated low-amplitude zones, the buried mounded structures and the areas where a BSR was interpreted. Additionally, other non-seismic evidences of leakage exists in the Malvinas Basin, including indications of thermogenic gas from isotopic analysis of gas in piston cores and oil slicks (Petrobras internal reports), (Fig. 4).

4.1 The central part of the basin:

We observe several vertically-elongated features with low-amplitude zones and a diffuse-to-chaotic seismic pattern in the central part of the basin, overlying a deep basement graben (area I in figure 4), (Figs. 5, 6). These features extend very close to the seafloor and their base can often be traced down to the upper limit of a polygonal fault interval (Fig. 6). In some cases there is no clearly visible root. Their vertical-length is at least 500 to 800 ms (twt), and their width is between 700 and 2400 m (Fig. 6). The shapes are typically cylindrical to conic. Several high-amplitude reflection anomalies can be observed in the upper parts of these vertically-elongated features or adjacent to them (Figs. 5, 6). In the surrounding areas, several enhanced amplitudes also occur along particular stratigraphic levels. These can extend laterally up to some hundreds of meters to kilometres (Fig. 5).

A few v-shaped depressions are observed on the seafloor in the area where the enhanced amplitudes and the vertically-elongated features occur, with some of them located directly above them (Figs. 5, 6). Enhanced amplitudes near the vertically-elongated features are sometimes underlain by a zone of reduced amplitudes. In places, stacked v-shaped depressions are observed within the vertically-elongated features (Fig. 6). Other enhanced amplitude anomalies present a phase reversal compared to the neighbouring stratigraphic layers (Fig. 6).

Features in area I occur within the Pleistocene to recent sedimentary succession (Figs. 5, 6), located above a Miocene-Pliocene polygonal faulted interval (Figs. 5, 6). The lower part of

this faulted interval is identified as over-bank sediments, probably associated with a nearby Miocene channel-levee-system from lowstand deposits (Galeazzi, 1998, Weimer, 1990). Above the over-bank sediments, a Pliocene elongated mounded feature similar to a contourite deposit is identified (Fig. 5). Below the area of the observed features, within the Cretaceous sediments, we have identified an up to 80 km wide fan body of the Mid. Inoceramus Fm. (Fig. 5). By examining several seismic lines we observe that this fan progrades towards the SW. The progradational fan front dips towards the SE. The whole fan body is located between about 1.5 and 2.0 s (twt) and the progradational fan front is located at approximately 1.75 - 2.5 s (twt). The most prominent features observed in area I are located above the fan front. Both the Mid-Cretaceous Middle Inoceramus Fm. and the Upper Cretaceous sedimentary succession deposited above the Mid Inoceramus fan body are characterized by a highly chaotic and disturbed seismic pattern with relatively low-amplitudes and locally enhanced reflectors. Both intervals are disrupted by polygonal faults (Fig 5).

4. 2 The southern part of the basin:

Several vertically-elongated features with low-amplitude zones and a diffuse-to-chaotic seismic pattern are also identified in the central-southern part of the Malvinas Basin, where the basement reaches its greatest depths in front of the deformation front (Fig. 4, area IIa and Fig. 7). Some similar features have also been observed in the Austral-Magallanes Basin (Fig. 4, area IIb). They are situated either above deep-rooted Miocene/Pliocene thrust faults of the deformation front or above Eocene/Miocene normal faults (Fig. 7).

The vertical zones occur in the upper stratigraphic column, within the Pliocene-Recent sediments. With variable sizes they exhibit an average vertical length of 300 to 1000 ms (twt) and reach maximum depths of up to 2.5 s (twt). Their widths range between 300 and 1200 m, with the exception of one feature that has a width of 4.5 km (Figs. 8, 9). Almost all of these features reach up to a distinct level below the seafloor, terminating at a high-amplitude

anomaly (Fig. 8.). Below these enhanced reflections the signal is deteriorated or blanked. Stacked v-shaped depressions can often be observed within the vertical features and single v-shaped depressions are identified along stratigraphic layers or within the Pliocene to recent sedimentary interval in depths ranging from 0.85 to 2.25 s (twt) (Figs. 7, 8, 9).

In the area of the deformation front, the deteriorated signal can often be followed down to the upper termination of the deep rooting thrust faults (Figs. 7, 8, 9). Some of the high-amplitude anomalies show a phase reversal compared to the seafloor (Fig. 8). This level mimics the seafloor morphology and occurs in a water depth of 690 ms (twt) (about 500 m, assuming a seawater velocity of 1450 m/s) and at a depth of 200 ms (twt) below the seafloor (about 170 m ± 5 m below the seafloor assuming an average sediment velocity of 1700 m/s ± 50 m/s). The zone above this level shows very low to transparent amplitudes (Figs. 7, 8). Additionally, above the phase-reversed, enhanced reflections a zone of amplitude variations and reduced amplitudes is observed up to the seafloor (Figs. 7, 8, 9).

We also identified a very broad diapir-like structure in area IIa (Fig. 9). This feature is located at 500 m water depth and is considerably larger (with a width of 3.5 to 4.5 km) than all vertically-elongated features observed in areas IIa and IIb. The top of this structure is located 65 ms (twt) below the seafloor (approximately 55 ± 2 m, assuming an average sediment velocity of 1700 ± 50 m/s). The reflections at the top of the structure show a phase reversal compared to the seafloor reflection, which itself exhibits anomalously low amplitudes above this feature (Fig. 9). In the uppermost 500 ms (twt), pull-down effects can be observed within the structure. Deeper than the uppermost 500 ms, no layering is visible and the internal signal is completely distorted and deteriorated – its base is not visible.

Calculations of the geothermal gradient were made for an assumed BGHSZ at the level where both phase-reversed reflection anomalies occur. As explained in the methodology this was calculated for ocean bottom temperature of 4.2 ± 0.2 °C. The observed phase-reversed

enhanced reflection showed in figure 8 would then correspond to the BGHSZ if the geothermal gradient is 23.9 ± 2.0 °C/km (Fig. 9c).

On the other hand, the observed phase-reversed enhanced reflection above the broader diapir-like feature shown in figure 9a and b would correspond to a geothermal gradient of 43.5 ± 2.0 °C/km if they are considered as an upwardly shifted BGHSZ (Fig. 9c).

The vertically elongated features can be classified as 1) features located to the NW of the deformation front and above the deeply- rooted Eocene/Miocene normal faults, and 2) features overlying the thrust faults of the deformation front (Fig. 7). This latter type also occurs in the neighbouring Austral-Magallanes Basin (Fig. 4). In general, the frequency of observed vertically-elongated features decreases towards the NW in the basin.

4.3 The eastern part of the basin:

We could observe a few straight vertically-elongated features, with a reduced amplitude and a diffuse-to-almost-chaotic internal seismic pattern at the southwestern flank of the Malvinas Islands (Fig. 4, area III). These features are found within the Upper Cretaceous–Recent sediments overlying a Mid-Cretaceous progradational fan body of the Lower Inoceramus Fm. (Richards et al., 2006), (Fig. 10). They are about 0.7 - 2.5 s (twt) long and approximately 1 - 1.4 km wide. They reach, or are very close to, the seafloor. They have a conic to straight shape with diffuse lateral boundaries. The most prominent feature corresponds to one previously reported by Richards et al. (2006), (Fig. 10). It has a total length of about 2.5 s (twt), while the eastern features have a length of only 0.7 to 1.5 s (twt). Stacked v-shaped depressions can be distinguished within the internal structure. Below the westernmost prominent feature, late Jurassic-early Cretaceous normal faults are found and the basin is relatively deep. Whereas towards the east, the basement rises up to 2.5 s (twt) and has several normal faults, which reach up to the lowermost Cretaceous.

4. 4 The western part of the basin:

We have identified a series of mounded structures buried within the relatively thin Paleocene-Eocene unit (Figs. 11, 12), and located south and southwest of the Rio Chico High (Fig. 4, area IV). The Paleocene-Eocene unit thickens from 50 ms (twt) in the north up to 400 ms (twt) in the south. Some other buried mounds are also found in the overlying Miocene succession (Fig. 12). These structures are about 50 - 300 ms (twt) high (approximately 50 – 250 m) and 600 -1600 m wide, although other less abundant and smaller mounds, about 100 m wide, where also identified. One interesting observation is that these structures are mostly located above basement normal faults or structural highs and stratigraphic features like strata truncations (Fig. 11). The Eocene layers lap onto the mounds (Figs. 11, 12). The morphology is predominantly symmetrical and internally well stratified, but some may be asymmetrical, displaying prograding internal reflections (Fig. 12). These mounds often occur in clusters of 4 to 10, and the highest density is observed along a NW-SE axis in the SW edge of the Rio Chico High (Fig. 4). Below the largest mounds, the seismic signal is reduced and the stratification is not clearly visible, although occasionally local pull-ups can be observed (Fig. 11). The well Lapa penetrated a mound at 1320 m depth and the cutting samples were described as micritic limestones, locally dolomitized, associated with abundant fragments of echinoid spines, bryozoan colonies, and gastropod shells (Galeazzi, 1998, Petrobras internal reports). Samples from the well Merluza, drilled about 2.5 km from two of the mounds, show calcitic fragments and pyrite minerals in depths of about 1060-1100 m within a glauconitic sandy environment (internal well report).

5. Interpretations

Based on their seismic character and geometry we interpret the vertically-elongated features with reduced amplitudes observed in area I, IIa/b and III as seismic pipes and the enhanced

amplitude anomalies as bright spots indicating the presence of gas. Hence, each area corresponds to an active leakage population (Judd and Hovland, 2007). The low amplitude areas of the seismic pipes indicate active gas leakage. The low amplitudes are most likely caused by the partial saturation of gas within the sediments (Løseth et al., 2009). The v-shaped seabed depressions in areas I and IIa are interpreted as seafloor pockmarks produced by blow out events (Figs. 6, 8). If the pockmarks are not linked to underlying pipes they are interpreted as paleo pockmarks derived from a past, no longer active, blow-out event (Hovland and Judd, 1988, Judd and Hovland, 2007). If the pipes have a root within the polygonal faulted interval they are interpreted as a part of a seal-bypass system (Cartwright et al., 2007). Some pipes in area I are rooted in the polygonal faulted interval but also linked to seafloor pockmarks, indicating a seal-bypass system and a recent escape event (Cartwright et al., 2007). However, some pipes in areas I and II situated above the polygonal faulted interval do not show a clear root in this interval, this could be explained by a diffusive flow through the polygonal faults as described by Berndt et al. (2003). The same process is interpreted for rootless pipes near the deformation front in area IIa/b, overlying deeper faults of the deformation front (Figs. 7, 8, 9). The diffusive flow presumably becomes more focused, due to failures of the stratigraphic trap (Berndt et al., 2003). Conversely, the pipes rooted in the deep faults of the deformation front would result from focused fluid flow out of the faults crest (Løseth et al., 2009). The interpretation of the vertically-elongated features as pipes in area III remains uncertain, because of the weak and low quality of the seismic signal (Fig. 10). Only the gas chimney identified previously by Richards et al. (2006) is clearly visible. The pipes could be rooted within the Mid Inoceramus fan, but a leakage mechanism is uncertain. One possibility could be focused fluid flow out of an overpressured reservoir fan wit hydro-fractures providing leakage pathways through the sealing cap-rock (Løseth et al., 2009).

403 The stacked v-shaped depressions observed in some of the pipes in all areas are most likely
404 caused by velocity pull-down effects due to the presence of gas (Løseth et al., 2009). The
405 blanked zones below the bright spots (Figs. 6, 8, 9) probably result from the absorption or
406 scattering of acoustic energy by the presence of gas in the sediments. A similar interpretation
407 is given to the blanked zones below the seafloor in area I, which are most likely related to the
408 presence of shallow gas below the seafloor (e.g. Schroot, et al., 2005). The phase-reversed
409 enhanced reflections, which underlie a blanked zone and replicate the seafloor morphology
410 are interpreted as bottom simulating reflectors (BSR) (Figs 7, 8, 9).
411 The level where these reflections are located corresponds to a BGHSZ (Hyndman and Davis,
412 1992, Hyndman and Spence, 1992), from which geothermal gradient of 23.9 ± 2.0 °C/km was
413 calculated. The BSR distribution map (Fig. 4) shows that this gas hydrate stability zone is
414 located at the deepest part of the study area. Where the BSR disappears, patchy high
415 amplitudes anomalies occur below the observed blanking level. This blanked area may
416 represent gas hydrates cemented in the sediments, resulting in a reduced impedance contrast
417 between layers (Lee and Dillon, 2001) and/or the presence of shallow gas accumulations
418 below the seafloor, which can also reduce the seismic signal (Schroot et al., 2005). The thin
419 low amplitude pipes observed above the BSRs up to the seafloor (Fig. 8) could be evidence of
420 fluids and gas breaching up to the seafloor. The upward migrating hot fluids along deeply-
421 rooted faults bringing heat from the deeper parts of the stratigraphic section to higher levels
422 could change locally the stability conditions of the GHSZ. Above the conduits, heat would
423 dissociate the gas hydrates and increase the amount of gas, which would promote the
424 generation of BSRs (Holbrook et al., 1996). Alternatively, gas from deep parts of the section
425 could preferentially migrate upwards along faults. These mechanisms could explain why the
426 BSRs are exclusively located above the area with deep rooting faults (Figs. 7, 8, 9). The local
427 dissociation of the gas hydrates by increased temperatures could lead to the development of
428 leakage pathways for gas and fluids through the otherwise sealing GHSZ. Similar

observations have been made in other areas, e.g. at the Cascadia margin off the coast of Vancouver Island (Wood et al., 2002), or offshore Korea, where they have been referred to as "hydrate-choked chimneys" (Haacke et al., 2009). In some areas where BSRs are observed, an amplitude variation is visible at the seafloor (Figs. 8, 9). The suppressed amplitudes of the seafloor reflector might be explainable by partial gas saturation of the seafloor sediments (Crutchley et al., 2010) and the amplitude suppression within the GHSZ could be related to amplitude and signal reduction caused by the presence of gas (Løseth et al., 2009). However, this interpretation is made tentatively, because processing parameters could have compromised true amplitudes in this area of the GHSZ and the seafloor.

The phase-reversed enhanced reflections above the diapir-like feature (Fig. 9) are most likely also the result of gas accumulations below gas hydrates. The BGHSZ seems to be upwardly shifted compared to the BGHSZ in the surroundings. If these reflectors represent an upward shifted BGHSZ, a higher geothermal gradient of 43.5 ± 2.0 °C/km is required (Fig. 9c), approximately 19.6 ± 2.0 °C/km higher than the estimated geothermal gradient for the deeper BSR in the surrounding areas. We suggest that a local upward shift of the pressure/temperature equilibrium boundary by upward migrating hot fluids could be responsible for this.

The diapir-like feature could be therefore interpreted as a mud diaper, or an initial stage in the evolutionary development of a mud volcano conduit (Cartwright et al., 2007), allowing the migration of hot fluids from greater depths in this localized area. The theoretical conditions for blow out pipes and for mud volcano conduits are similar (Karakin et al., 2001). Local heat flow anomalies have been reported in the geologically similar Austral-Magallanes Basin on Tierra del Fuego, above and close to the San Sebastian oil and gas field (Uyeda et al, 1978, Zielinski and Bruchhausen, 1983). Uyeda et al. (1978) reported a geothermal gradient of 32 °C/km and Zielinski and Bruchhausen (1983) reported 34.6 ± 2.5 °C/km. Upward fluid migration was proposed to bring up heat from depth, which increases the steady state

455 geothermal gradient, which is supposed to be 20.0 °C/km on Tierra del Fuego (Zielinski and
456 Bruchhausen, 1983). A similar geothermal gradient of 21.5 ± 2.0 °C/km was also obtained
457 from the well Unicorno located offshore Tierra del Fuego (Fig. 3). This value was estimated
458 from not corrected bottom hole temperatures. The range of our calculated values is higher
459 than the reported values, but the increase of the geothermal gradient of 19.6 ± 2.0 °C/km is
460 similar to the increase on Tierra del Fuego, where increases of 12 and 14.4 ± 2.5 °C/km have
461 been reported (Uyeda et al, 1978, Zielinski and Bruchhausen, 1983). Areas of mud diapirism
462 can increase the geothermal gradient by up to a factor of two to three (e.g. Shyu et al., 1998;
463 Lüdmann and Wong et al., 2003), supporting our interpretation of an upward shifted BGHSZ
464 induced by a local heat flow anomaly.
465 An alternative mechanism for uplifting the BGHS would be rapid uplift of the seafloor caused
466 by tectonic activity. A recent tectonically-induced uplift in the range of tens of meters would
467 have reduced the pressure sufficiently to promote gas hydrate dissociation. The region is
468 tectonically active and primarily affected by wrench deformation (Ghiglione et al., 2010).
469 Tectonic uplift of a localized area with the width of 3-5 kilometres, similar to the observed
470 diapir structure, would be observable in the seismic data as an elevated fault block. We do not
471 observe such a feature (Fig. 9) and therefore rule out this hypothesis.
472
473 **Interpretation of the buried Eocene mounded structures**
474 A previous interpretation of the buried mounded structures was proposed by Galeazzi (1998),
475 where they were interpreted as carbonate mounds. This interpretation is based on samples of
476 the well Lapa and on seismic observations of internal stratification and progradational
477 patterns in the mounds. Another strong argument in support of this is the observation of
478 pulled-up layers located below of some mounds, as increased seismic velocity by carbonate-
479 cemented sediments and carbonate itself may produce this effect (Løseth et al., 2009).
480 Further, Galeazzi (1998) interpreted these carbonate mounds as carbonate build-ups favoured

by warm waters coming from the northern South Atlantic and by a Paleocene/Eocene warm climate period with a climate maximum at the early Eocene, which might have increased global water temperatures. We confirm the presence of seismic pull-ups (Fig. 11) as a result of the carbonate, which is also supported by the observation of reduced amplitudes and chaotic reflections below several of the mounds (Fig. 11, 12). We think that these structures are associated with MDAC. This interpretation is supported by the reported onset of hydrocarbon generation in the Eocene, and that in our study area, the presence of pyrite is confirmed in the well Merluza (internal well report) close to two buried mounded structures and dolomite has been found in the well Lapa (Galeazzi, 1998). Both observations support the interpretation of MDAC generation, because authigenic carbonate build-ups contain pyrite (Lein, 2004) and are often associated with dolomite (e.g. León et al., 2007).

Another explanation for the carbonate mounds is that they are a combination of MDAC and contourite deposits. Contourite depositional systems and giant mounded drifts associated with a BSR and hydrocarbons accumulations have been observed on the Argentinean slope and margin (Hernández-Molina et al., 2009, 2010). These are associated with the influence of strong water currents of Antarctic water masses associated with the opening of the Drake Passage and the generation of a strong Antarctic bottom water current at the Eocene-Oligocene boundary (Hernández-Molina et al., 2009, 2010). It is possible that water influxes from the Pacific into the South Atlantic existed before the opening of the Drake Passage from 50 Ma onwards (Livermore et al., 2005; Lawver and Gahagan, 2003). During this phase of early rifting, a shallow or intermediate depth oceanic circulation between the Pacific and South Atlantic ocean could have been established for the first time (Eagles et al., 2006). This might have produced a strong current similar to the Malvinas Current observed nowadays (Hernández-Molina et al., 2010), which could have generated mounded drifts. However, all

506 the mounds reported by Hernández-Molina et al.(2010) from the Argentine continental
507 margin are elongated and have lengths of up to 250 km.
508 Our observed drift mounds could have developed MDAC as carbonate cemented sediments
509 and dolomite crusts during hydrocarbon leakage in the Eocene. Most of the mounded
510 structures observed are above early Cretaceous basement faults or above basement highs and
511 within the Eocene sedimentary succession (Figs. 11, 12), indicating a possible relationship
512 between leakage pathways, an Eocene onset of leakage, and contourite development.
513 Additionally, the location of the mounds parallel to and along the left side of this possible
514 proto Malvinas Current, and the observation of progradation (Fig. 12), would favour this
515 interpretation. After 43-39 Ma the Drake Passage opened (Scher and Martin, 2006) with a
516 proto Drake Passage at around 43 Ma generating the first deep Antarctic Circumpolar
517 Current. Influences of strong currents in this area decreased and mounds only exist until the
518 lower Miocene. However, the seismic pattern and size of the observed giant mounds of
519 Hernández-Molina et al. (2010) differ from our mounds. They are internally bounded by
520 unconformities and they are tens to hundreds of times larger than the examples of carbonate
521 mounds mentioned in the introduction.
522
523 Other possibilities, which are associated with carbonate mound structures, such as MDAC
524 associated with mud volcanism (e.g. León et al., 2007) or deep water coral reefs grown on
525 authigenic carbonate hard-grounds (e.g. Ivanov et al., 2010) can be ruled out because no mud
526 volcanoes or corals have been observed and there was no development of a deepwater
527 environment during that time (Galeazzi, 1998).
528

6. Discussion

6.1 Possible origin of fluids and driving mechanisms of active leakage

Area I

We discuss three main possibilities regarding the origin of the fluids and gas:

1) Thermogenic gas could be leaking vertically from the Springhill Fm., which is the main reservoir of the active petroleum system (Figs. 2, 13). This unit is located below the sealing Lower Inoceramus Fm., which is considered to be a Kerogen type II source rock and the main source rock of the petroleum system (Galeazzi, 1998). This source rock is buried to depths of approximately 1.6 to 2.8 km (1.75 to 2.75 s (twt), assuming an average velocity of 1800 m/s). Based on our calculated geothermal gradient (23.9 ± 2.0 °C/km), it can be assumed that the unit just entered the oil window at the deepest locations in the area I. In general, the oil window starts at approximately 60 °C for a source rock with type II kerogen (Tissot and Welke, 1984). A mature Inoceramus source is, however, most likely located further southeast in the main depocenter underlying the area IIa/b (Fig. 4). The source rock has likely reached elevated levels of maturity towards the southeast. Long range secondary migration along the underlying Springhill Fm. could focus petroleum towards the basin margins. Here leakage along fractures crosscutting the Springhill and Lower Inoceramus Fm. could provide leakage pathways to the area I (Løseth et al., 2009). Some deeper normal faults exist below the leaking area in depth of about 1.75 to 3.0 s (twt) (Fig. 5). These crosscut the Springhill and Lower Inoceramus Fm. They likely provide leakage pathways into the progradational fan of the Middle Inoceramus Fm. (Figs. 5, 13). We propose that the polygonal faults observed in the mid and upper Cretaceous and in the Miocene/Pliocene sedimentary succession then provide seal bypass systems (Cartwright et al., 2007), which allow gas and fluids to migrate upwards.

553 The other possible source rock interval is the organic-rich black lacustrine shale within the
554 Tobífera Fm. that has been reported for the Austral-Magallanes Basin (Fig. 2) (Bravo and
555 Herrero, 1997; Pittion and Gouadain, 1992). Almost all of the pipes in area I are located
556 above a deep basement graben, which deepens up to 5 s (twt) (Figs. 4, 13). Using the
557 calculated geothermal gradient of 23.9 ± 2.0 °C/km derived from the BSR depth, this depth
558 would be sufficient to get the source rock into the oil and gas window. In this scenario, a
559 vertical migration of hydrocarbons and fluids along faults and through less permeable layers
560 up to the Springhill Fm. reservoir may be possible. Further vertical migration into the upper
561 levels would be as described above.
562
563 2) Another possibility is a long-range lateral migration of fluids and dissolved gases. The
564 origin of the fluids would be in the deeper part of the deformation front located 80 km to the
565 south (Figs. 4, 13) in depths of more then 5 s (twt) (Fig. 7) (approximately 4.5 km, assuming
566 an average velocity of 1800 m/s). Fluids and Hydrocarbons from the Springhill Fm. reservoir
567 or Miocene turbidites reservoirs would be mobilized by the compressional regime and migrate
568 upwards along the deeply-rooted thrust faults at the deformation front and then possibly
569 laterally (Fig. 13). Some fluids may leak near the seafloor, guided by faults terminating close
570 to the seafloor. Other fluids likely migrated further, laterally up dip through the Miocene
571 permeable layers until they reached the Miocene polygonal faulted interval where they could
572 ascend vertically (Fig. 13). An upward migration along more permeable, upwardly dipping,
573 Pleistocene stratigraphic layers could also be possible.
574 Although such a long-range migration of 80 km and more may seem difficult to conceive,
575 particularly for gas, Pittion and Gouadain (1992) pointed out that the distances between the
576 hydrocarbon kitchens and the discovered reservoirs in the neighbouring Austral-Magallanes
577 Basin are in the range of 20 to 150 km for oil and 60 - 200 km for gas. The observation of oil
578 slicks and thermogenic gas in the uppermost sediments at the shallower edge of the Malvinas

579 Basin (Fig. 4) away from the proposed hydrocarbon kitchen also supports the notion of long
580 distance migration in the Malvinas Basin.
581 3) Biogenic gas contributions should not be neglected. Biogenic gas generation from organic
582 rich shales is favoured in shelves and deepwater settings, where it can be generated at very
583 shallow sediment depths in the range of centimetres up to more than 1000 m depth (Rice,
584 1993). Generation of biogenic methane can be summarized as the reduction of CO_2 into
585 methane (Judd and Hovland, 2007). This process requires both high sedimentation rates of at
586 least 200 m/Ma, and a minimum of 0.5% total organic carbon (TOC) in the sediments
587 (Clayton, 1992). Additional conditions required are anoxic and low-sulfate environments, low
588 temperatures, type III/II organic matter and sufficient pore space (Rice, 1992).
589 The top of the Pliocene is buried to approximately 0.5 - 0.75 s (twt) in the area where the
590 pipes occur (Figs. 5, 6, 13). This is equivalent to roughly 425 - 640 m below seafloor (using
591 an average sediment velocity of 1700 m/s). The estimated sedimentation rate for the Pliocene-
592 Recent sedimentary interval is around 170 - 250 m/Ma, which is at the minimum possible
593 range for favouring biogenic gas generation. The Pleistocene-Recent litoral marine deposits
594 on Tierra del Fuego consist of gravel, sand, silt, and shell limestone (Olivero and Malumian,
595 2008), which indicates a succession coarser than the Pliocene and Miocene successions. The
596 pore space therefore should be large enough for biogenic gas generation (Rice, 1993). Lateral
597 facies variations can be assumed by the observed progradational pattern of the Pleistocene-
598 Recent interval (Tassone et al., 2008). Although we do not have reports of increased TOC or
599 anoxic/sulfate conditions in the Pliocene to Recent sediments, we cannot rule out their
600 existence. However, in our opinion, this is very unlikely since the burial depth, sedimentation
601 rate and temperatures are only very marginally within the biogenic gas window. Therefore,
602 we favour a thermogenic origin for the migrating gas, most likely sourced by lateral migration
603 from the deformation front, although a combination of both leaking deep-thermogenic gas and
604 shallow biogenic gas could also be possible.

Area II a/b

The origin of fluids and gas of the pipes in area IIa/b is most likely the Springhill Fm. as pore fluids, gas and oil can migrate upwards along the deeply- rooted faults from the deformation front and Eocene/Miocene normal faults (Figs. 7, 8, 9, 13). Migration pathways of fluids along older normal faults and thrust faults could be explained by the overall compressional regime, caused by tectonic shortening and sediment overburden. These structures crosscut the Springhill Fm., providing pathways to the upper stratigraphic levels. Once fluids and gas reach the upper stratigraphic levels, they could charge Miocene turbidite channel reservoirs or be trapped below low permeability fine-grained sediments. At the Miocene stratigraphic level, fine-grained sediments dominate, aside from the sandy channels (Yrigoyen, 1989, Galeazzi, 1998), and fluid migration through these low permeable sediments is likely difficult. Once fluids reached the Miocene level, the polygonal faulted interval located at the top of the Miocene succession (Figs. 7, 8) likely provided a seal-bypass system for fluids and gas (Cartwright et al., 2007) or possible diffusive leakage out of polygonal faults (Berndt et al., 2003).

Fluids in pipes located directly above the deformation front are sourced either directly from the fault terminations as focused flow, or from diffusive flow out of the fault planes. The fluids are most likely directly linked with the charged Springhill Fm. reservoir, which is located below the sealing main Kerogen type II source rock interval, the Lower Inoceramus Fm. (Galeazzi, 1998). It is buried to depths of up to 3.6 - 6.5 km (calculated from 3.5 to 6 s (twt) and an average velocity of 2100 m/s taken from our velocity model). Based on our calculated geothermal gradient of 23.9 ± 2.0 °C/km, it can be assumed that the source rock has entered into the oil and gas window (Tissot and Welke, 1984).

Biogenic production of methane as a main source for methane can be ruled out since isotopic analysis of gas from piston cores indicates a thermogenic origin (Fig. 4), (Petrobras personal communication).

The limited distribution of area IIa/b could be explained through two possible hypotheses. 1) All the identified pipes in area IIa have been observed in the most recent 2D seismic surveys (from year 1998), which have the highest resolution and best quality, but end to the east of the basin (Fig. 3). To the west the seismic coverage is also very dense, but of lower resolution and quality (older surveys), which could have masked the presence of leakage features in that area, except for area IIb in the Austral-Magallanes Basin, where surveys from the year 1994 were used.

2) Another possible explanation may be that there is a link between the deepest parts of the basement and the distribution of the pipes in area IIa, since most pipes in area IIa are located above the deepest areas of the basin; associated with basement depths of about 5 - 8 s (twt) (Fig. 4) where the source rock will have the highest maturity. The leakage features found in the Austral-Magallanes Basin in area IIb are found above shallower basement depths at about 2 - 3 s (twt) (Fig. 4). They are most likely linked with the petroleum system of the Austral-Magallanes Basin.

Area III

The origin of fluids feeding pipes in area III seems to be a Mid-Cretaceous fan system located exclusively at the eastern part of Malvinas Basin. It is a NW-SE elongated sedimentary body prograding from the Malvinas/ Falkland Islands towards the SW into the Malvinas Basin. It is bounded at the top and its base by two prominent reflectors, which can be traced over the entire basin (Figs. 5, 7, 10, 11). The top is represented by the base of the Upper Inoceramus Fm. and at the base is the top of the Margas Verdes Fm. (Fig. 10). The prograding fan consists most likely of clastic-dominated sediments derived from possible Paleozoic quartz-rich

sedimentary rocks located in the hinterlands (Richards et al., 2006). A single interpreted pipe located at the toe-set sandstones of the fan system has been identified by Richards et al. (2006). Although no well information exists regarding the lithologic composition of the Middle Inoceramus Fm. in this area, the fan of the Middle Inoceramus Fm. may contain sandy reservoirs (Richards et al., 2006) charged by hydrocarbons generated from the main source rock interval the Lower Inoceramus Fm. or by the minor source rock interval of the Margas Verdes Fm. (Galeazzi, 1998). The oil kitchen is located towards the S and SW, in the deeper part of the basin as discussed above (area IIa/b). After the hydrocarbons have migrated into the Middle Inoceramus Fm. reservoirs along thrust faults of the deformation front, they could migrate laterally updip (Fig. 14).

We considered the possibility that leakage out of the main Springhill Fm. reservoir could also be possible in much the same manner as described for pipes in area I (Fig. 4). As for pipes in area I, basement faults crosscutting the Springhill Fm. could provide migration pathways to the Middle Inoceramus Fm. and provide leakage pathways. However, no deep rooting faults are visible in the seismic line in the area where the pipes occur (Fig. 10). Only in the east, some faults cut through the sealing formations and the Springhill Fm. reservoir, but in this area no pipes have been recognised and the faults are too far from the observed pipes in the west (Fig. 10). Therefore, leakage out of the Springhill Fm. reservoir can probably be discounted. Leakage most likely occurs out of the prograding fan of the Middle Inoceramus Fm. We therefore propose that pipes in area III are the result of focused fluid flow induced by a hydro-fractured cap-rock above an overpressured fan reservoir.

6.2 Origin of fluids for authigenic carbonate generation in the Eocene

The origin of the seeping hydrocarbons could be leaking from the Springhill Fm. reservoirs. The Lower Inoceramus Fm. source rock could have generated oil and gas from Eocene times

in the southern regions where the basin developed a deep trough during the Eocene and the source rock entered into the oil window during that time (Galeazzi, 1998). Hydrocarbons would be able to migrate into the Springhill Fm. reservoir. On regional basement highs, where the Springhill Fm. pinches out or at basement fault controlled traps, hydrocarbons trapped below the sealing Lower Inoceramus Fm. cap-rock may have accumulated during the Eocene. Leakage through this sealing formation could occur by capillary leakage, overpressure or along tectonic fractures (Løseth et al., 2009). For instance, several of the basement normal faults continue up to the early Cretaceous, crosscutting the Springhill Fm. and provide tectonically fractured pathways to upper stratigraphic levels, making leakage possible.

We think the link between timing of carbonate mound generation, timing of hydrocarbon generation and possible leakage is very strong, because the mounds are mostly above structural basement highs or faults, which provide favourable pathways for hydrocarbon leakage and therefore favourable conditions for MDAC generation.

7. Summary and Conclusions

We have identified several active, recent and possible paleo hydrocarbon leakage indicators in the Malvinas Basin. Active leakage indicators include pipes, pockmarks, and high amplitude reflection anomalies. Possible paleo leakage indicators include buried Paleocene/Eocene and some Miocene mounds interpreted as MDAC mounds.

The active and paleo leakage indicators have different controlling mechanisms, distributions and seismic patterns. Most of them are controlled by different structural mechanisms.

Based on our observations, we propose four different areas (area I-IV) of active and past leakage indicators in the Malvinas Basin.

Area I is an active-leakage population, which contains seismic anomalies manifested as pipes originating above or within a polygonal faulted Pliocene-Miocene interval. Pipes of area I are accompanied by high amplitude reflection anomalies and seabed pockmarks located in the centre of the Malvinas Basin. The origin of the hydrocarbons is either thermogenic, biogenic or a combination of both.

Area IIa/b is an active-leakage population located in the south. It consists of pipes either located in or above thrust faults of the deformation front, or above deeply-rooted Eocene/Miocene basement normal faults. The gas chimneys are accompanied by high amplitude reflection anomalies and paleo pockmarks. In area IIa we also identified a BSR that is locally uplifted, indicative of a local disturbance of the base of gas hydrate-bearing sediments. The origin of the hydrocarbons in this area is most likely thermogenic.

Area III is an active-leakage population and consists of seismic-blanking anomalies and pipes originated from a Mid-Cretaceous deltaic-fan front. This population is located at the eastern edge of the Malvinas Basin. The origin of the hydrocarbons is most likely thermogenic.

Area IV is a possible paleo-leakage population consisting mostly of buried Eocene and some Miocene mounded structures located southeast of the Rio Chico High. They are mostly located above basement highs and faults and some stratigraphic pinch outs. They are interpreted as MDAC mounds derived from oxidation of thermogenic methane that leaked upwards along basement-rooted Lower Cretaceous faults.

The gas source of the leakage indicators in areas I, IIa/b and IV is most likely from the uppermost Jurassic-Barremian reservoir of the Springhill Fm., although a biogenic gas source in area I can not be ruled out. Leakage indicators in area III are probably sourced directly from Mid-Cretaceous sediments of the Middle Inoceramus Fm.

Based on the BSR depth in area IIa, we could calculate a geothermal gradient of 23.9 ± 2.0 °C/km. Gas hydrate dissociation and gas leakage to the seafloor through the GHSZ could be possible along migration pathways generated by ascending fluids and heat from the

deformation front faults. A local increased geothermal gradient of up to 43.5 ± 2.0 °C/km was calculated from the locally-uplifted BSR. The identification of a significant number of hydrocarbon leakage indicators previously unknown in the Malvinas Basin indicates the existence of an active petroleum system, including gas hydrate deposits.

Acknowledgments

We acknowledge the support of Eduardo Vallejo (Petrobras S.A.) for his valuable help on the implementation of this project. Petrobras Argentina S.A. is thanked for providing the data and allowing publication. We like to thank the editors Dr. Aurélian Gay, Dr. Christian Berndt, and Dr. Zahie Anka for their work on this special issue. We like to thank also the two reviewers Dr. Luis Somoza and Dr. Gareth Crutchly for their thoughtful input and suggestions that improved this manuscript. This research is funded by the Helmholtz Association's Initiative and Networking Fund in the framework of Z. Anka's Helmholtz-University Young Investigator Group.

Appendix A:

The table 1 is showing the geographic coordinates of the measured ocean water temperatures at 500 m water depth from the NOAA online database (Locarnini et al., 2010), which were used to estimate the ocean bottom temperature at the area of the observed BSR.

Latitude	Longitude	Ocean temperature measured at 500 m depth [℃].
-53.3703	-63.3726	4.035
-53.3717	-63.1258	4.339
-53.6293	-63.3729	3.877
-53.6228	-63.1299	4.292
-53.6224	-62.8717	4.521
-53.8741	-63.131	4.252

Table 1: Geographic coordinates in decimal degrees (WGS 1984) of measured ocean water temperatures at 500 m water depth.

8. References

Amante, C., Eakins, B.W., 2009. ETOPO1 1 Arc-Minute Global Relief Model: Procedures, Data Sources and Analysis. NOAA Technical Memorandum NESDIS NGDC-24, 19.

Bangs, N.L.B., Sawyer, D.S., Golovchenko, X., 1993. Free gas at the base of the gas hydrate zone in the vicinity of the Chile triple junction. Geology 21 (10), 905–908.

Berndt, C., Bünz, S., Mienert, J., 2003. Polygonal fault systems on the mid-Norwegian margin: a long term source for fluid flow. In: van Rensbergen, P., Hillis, R.R., Maltman, A.J., Morley, C.K. (Eds.), 2003. Subsurface sediment mobilization. Geological Society of London, Special Publications 216, 283–290.

Biddle, K.T., Uliana, M.A., Mitchum, R.M, Fitzgerald, M.G., Wright, R.C., 1986. The stratigraphy and structural evolution of the central and eastern Magallanes Basin, southern South America. In: Allen, A., Homewood (Eds.), Foreland Basins. Blackwell Scientific Publications, London, International Association of Sedimentologist, Special Publication 8, 41–61.

Bravo, P., Herrero, C., 1997. Reservorios naturalmente fracturados en rocas volcánicas jurásicas, Cuenca de Magallanes, Chile. VI Simposio Bolivariano, Cartagena, I, 66-84.

776 Cartwright, J., Huuse, M., Aplin, A., 2007. Seal bypass systems. AAPG Bulletin 91 (8), 1141-
777 1166.
778
779 Cathles, L.M., Su, Z., Chen., D, 2010. The physics of gas chimneys and pockmark formation,
780 with implications for assessment of seafloor hazards and gas sequestration. Marine and
781 Petroleum Geology 27, 82-91.
782
783 Clayton, C., 1992. Source volumetrics of biogenic gas generation, in Vially, R., ed., Bacterial
784 gas: Paris, Editions Technip, 191-204.
785
786 Cowley, R., O'Brien, G.W., (2000). Identification and interpretation of leaking hydrocarbons
787 using seismic data: a comparative montage of examples from the major fields in Australia's
788 North West Shelf and Gippsland Basin. APPEA Journal, 40 (2000), 121–150.
789
790 Crutchley, G.J., Pecher, I.A., Gorman, A.R., Henrys, S.A., Greinert, J., 2010. Seismic
791 imaging of gas conduits beneath seafloor seep sites in a shallow marine gas hydrate province,
792 Hikurangi Margin, New Zealand. Marine Geology 272, 114-126.
793
794 Diraison, M., Cobbold, P.R., Gapais, D., Rossello, E.A., Le Corre, C., 2000. Cenozoic crustal
795 thickening, wrenching and rifting in the foothills of the southernmost Andes. Tectonophysics
796 316 (1-2), 91-119.
797
798 Eagles, G., Livermore, R., Morris, P., 2006. Small basins in the Scotia Sea: The Eocene
799 Drake Passage gateway. Earth and Planetary Science Letters 242, 343–353.
800
801 Galeazzi, J.S., 1996. Cuenca de Malvinas. In: Ramos, V.A., Turic, M. (Eds.), Geología y

802 Recursos Naturales de la Plataforma Continental Argentina. XIII Congreso Geológico
803 Argentino, 273-309.
804
805 Galeazzi, J.S., 1998. Structural and stratigraphic evolution of the western Malvinas Basin,
806 Argentina. AAPG Bulletin 82, 596–636.
807
808 Gay, A., Lopez, M, Cochonat, P. Sermondadaz, G, 2004. Polygonal fault-furrows system
809 related to early stages of compaction-Upper Miocene to present sediments of the Lower
810 Congo Basin. Basin Research 16, 101-116.
811
812 Gay, A., Lopez, M., Cochonat, P., Levache, D., Sermondadaz, G., Seranne, M., 2006.
813 Evidences of early to late fluid migration from an upper Miocene turbiditic channel revealed
814 by 3D seismic coupled to geochemical sampling within seafloor pockmarks, Lower Congo
815 Basin. Marine and Petroleum Geology 23 (3), 387-399.
816
817 Gay, A., Lopez, M., Berndt, C., Séranne, M., 2007. Geological controls on focused fluid flow
818 associated with seafloor seeps in the Lower Congo Basin. Marine Geology 244, 68-92.
819
820 Ghiglione, M.C., Quinteros, J., Yagupsky, D., Bonillo-Martínez, P., Hlebszevtich, J., Ramos,
821 V.A., Vergani, G., Figueroa, D., Quesada, S., Zapata, T., 2010. Structure and tectonic history
822 of the foreland basins of southernmost South America. Journal of South American Earth
823 Sciences 29, 262-277. doi: 10.1016/j.jsames. 2009.07.006.
824
825 Gradstein, F.M., Ogg, J.G., Smith, A.G., Agterberg, F.P., Bleeker, W., Cooper, R.A.,
826 Davydov, V., Gibbard, P., Hinnov, L., House, M.R., Lourens, L., Luterbacher, H.-P.,
827 McArthur, J., Melchin, M.J., Robb, L.J., Shergold, J., Villeneuve, M., Wardlaw, B.R., Ali, J.,

828 Brinkhuis, H., Hilgen, F.J., Hooker, J., Howarth, R.J., Knoll, A.H., Laskar, J., Monechi, S.,
829 Powell, J., Plumb, K.A., Raffi, I., Röhl, U., Sanfilippo, A., Schmitz, B., Shackleton, N.J.,
830 Shields, G.A., Strauss, H., Van Dam, J., Veizer, J., Kolfschoten van, T., Wilson, D., 2004. A
831 Geologic Time Scale 2004. Cambridge University Press, Cambridge.
832
833 Haacke, R.R., Hyndman, R.D., Park, K.-P., Yoo, D.-G., Stoian, I., Schmidt, U., 2009.
834 Migration and venting of deep gases into the ocean through hydrate-choked chimneys
835 offshore Korea. Geology 37 (6), 531-534. doi: 10.1130/G25681A.1.
836
837 Hernández-Molina, F.J., Paterlini, Violante, R., Marshall, P., M., de Isasi, M., Somoza, L.,
838 Rebesco, M., 2009. Contourite depositional system on the Argentine slope: An exceptional
839 record of the influence of Antarctic water masses. Geology 37, 507-510.
840
841 Hernández-Molina, F.J., Paterlini, M., Somoza, L., Violante, R., Arecco, M.A., de Isasi, M.,
842 Rebesco, M., Uenzelmann-Neben, G., Neben, S., Marshall, P., 2010. Giant mounded drifts in
843 the Argentine Continental Margin: Origins, and global implications for the history of
844 thermohaline circulation. Marine and Petroleum Geology 27 (7), 1508-1530.
845
846 Holbrook, W. S., Hoskins, H., Wood, W. T., Stephen, R. A., Lizarralde, D., 1996. Leg 164
847 Science Party: Methane hydrate and free gas on the Blake Ridge from vertical seismic
848 profiling. Science 273 (5283), 1840–1843.
849
850 Hovland, M. and Judd, A.G., 1988. Seabed Pockmarks and Seepages. Impact on Geology,
851 Biology and the Marine Environment. Graham & Trotman Ltd., London, 293.
852

853 Hovland, M., 1990b. Do carbonate mounds reefs form due to fluid seepage. Terra Nova 2, 8-
854 18.
855
856 Hovland, M., Gardner, J. V., Judd, A. G., 2002. The significance of pockmarks to
857 understanding fluid flow processes and geohazards. Geofluids 2 (2), 127–136.
858
859 Hyndman R.D., Davis, E.E., 1992. A Mechanism for the Formation of Methane Hydrate and
860 Seafloor Bottom-Simulating Reflectors by Vertical Fluid Expulsion. Journal of Geophysical
861 Research 97 (B5), 7025-7041.
862
863 Hyndman R., Spence, G., 1992. A Seismic Study of Methane Hydrate Marine Bottom
864 Simulating Reflectors. Journal of Geophysical Research 97 (B5), 6683-6698.
865
866 Ivanov, M., Mazzini, A., Blinova, V., Kozlova, E., Laberg, J.-S., Matveeva, T., Taviani, M.,
867 Kaskov, N., 2010. Seep mounds on the Southern Vøring Plateau (offshore Norway). Marine
868 and Petroleum Geology 27 (6), 1235-1261.
869
870 Judd, A. G., Hovland, M., 2007. Seabed Fluid Flow. Cambridge, UK, Cambridge University
871 Press, 475.
872
873 Karakin, A. V., Karakin, S. A., Kambarova, G. N., 2001. Movement of a mud mixture
874 through a mud volcano channel: Izvestiya. Physics of the Solid Earth 37, 817–824.
875
876 Lawver, L.A., Gahagan, L.M., 2003. Evolution of Cenozoic seaways in the circum-Antarctic
877 region. Palaeogeography, Palaeoclimatology, Palaeoecology 198, 11-37.
878

879 Lee, M.W., Dillon, W.P., 2001. Amplitude blanking related to the pore-filling of gas hydrate
880 sediments. Marine Geophysical Researches 22 (2), 101–109.
881
882 Lein, A., 2004. Authigenic carbonate formation in the Ocean. Lithology and Mineral
883 Resources 39 (1), 1-30.
884
885 León, R., Somoza, L., Medialdea, T., González F.J., Díaz-del-Río, V., Fernández-Puga, M.C.,
886 Maestro, A., Mata, M.P., 2007. Sea-floor features related to hydrocarbon seeps in deepwater
887 carbonate-mud mounds of the Gulf of Cádiz: from mud flows to carbonate precipitates. Geo-
888 Marine Letters 27, 237-247.
889
890 Livermore, R., Nankivell, A., Eagles, G., Morris, P., 2005. Paleogene opening of the Drake
891 Passage. Earth and Planetary Science Letters 236, 459-470.
892
893 Løseth, H., Gading, M., Wensaas, L., 2009. Hydrocarbon leakage interpreted on seismic data.
894 Marine and Petroleum Geology 26, 1304–1319.
895
896 Løseth, H., Wensaas, L., Arntsen, B., Hanken, N.-M., Basire, C., Graue, K., 2011. 1000 m
897 long gas blow-out pipes. Marine and Petroleum Geology 28 (5), 1047-1060.
898
899 Locarnini, R. A., Mishonov, A. V. Antonov, J. I. Boyer, T. P. Garcia, H. E. Baranova, O. K.
900 Zweng, M. M. Johnson, D. R., 2010. World Ocean Atlas 2009, Volume 1: Temperature. S.
901 Levitus, Ed. NOAA Atlas NESDIS 68, U.S. Government Printing Office, Washington, D.C.,
902 184.
903

Lüdmann, T., Wong, H.K., 2003. Characteristics of gas hydrate occurrences associated with mud diapirism and gas escape structures in the northwestern Sea of Okhotsk. Marine Geology 201, 269-286.

Magalhães, V.H., Pinheiro, L.M., Ivanov, M.K., Kozlova, E., Blinova, V., Kolganova., J., Vasconcelos, C., McKenzie J. A., Bernasconi, S.M., Kopf, A.J., Díaz-del-Río, V., González, F.J., Somoza, L., 2012. Formation processes of methane-derived authigenic carbonates from the Gulf of Cadiz. Sedimentary Geology 243-244, 155-168.

Micallef, A., Berndt, C., Debono, G., 2011. Fluid flow systems of the Malta Plateau, Central Mediterranean Sea. Marine Geology 284, 74–85.

Miles, P.R., 1995. Potential distribution of methane hydrate beneath the European continental margins. Geophysical Research Letters 22 (23), 3179-3182.

Moss, J.L.; Cartwright, J., 2009. The spatial and temporal distribution of pipe formation, offshore Namibia. Marine and Petroleum Geology 27 (6), 1216-1234.

Naeth, J., di Primio, R., Horsfield, B., Schaefer, R. G., Shannon, P. M., Bailey, W. R., Henriet, J. P., 2005. Hydrocarbon Seepage and Carbonate Mound Formation: a Basin Modelling Study From the Porcupine Basin (Offshore Ireland). Journal of Petroleum Geology 28 (2), 147-166.

Olivero, E.B., Malumian, N., 2008. Mesozoic-Cenozoic stratigraphy of the Fuegian Andes. Argentina. Geologica Acta, 6 (1), 5-18. doi: 10.1344/105.

930 Pittion, J.L., Arbe, H.A., 1999. Sistema petrolero de la Cuenca Austral. IV Congreso
931 Exploración y desarrollo de hidrocarburos, Mar del Plata, Actas I, 239-262.
932
933 Pittion, J.L., Gouadain, J., 1992. Source-rocks and oil generation in the Austral Basin.
934 13thWorld Petroleum Congress, Buenos Aires, Proceedings 2, 113-120.
935
936 Rice, D. D., 1992. Controls, habitat, and resource potential of ancient bacterial gas. In: Vially,
937 R. (ed.), Bacterial Gas. Paris, Editions Technip, 91-118.
938
939 Rice, D. D., 1993. Biogenic Gas: controls, habitat, and resource potential. In: Howells, D. G.
940 (ed.), The Future of Energy Gases. United States Geological Survey Professional Paper 1570,
941 583-606.
942
943 Richards, P., Duncan, I., Phipps, C., Pickering, G., Grzywacz, J., Hoult, R., Merritt, J., 2006.
944 Exploring for Fan and Delta Sandstones in the Offshore Falklands Basins. Journal of
945 Petroleum Geology 29 (3), 199-214.
946
947 Rossello, E.A., Haring, C.E., Cardinali, G., Laffitte, G.A., Nevistic, A.V., 2008.
948 Hydrocarbons and petroleum geology of Tierra del Fuego, Argentina. Geologica Acta 6 (1),
949 69-83. doi: 10.1344/105.000000242.
950
951 Scher, H.D., Martin, E.E., 2006. Timing and Climatic Consequences of the Opening of Drake
952 Passage. Science 312, 428-430.
953

Schroot, B.M., Klaver, G.T., Schüttenhelm, R.T.E., 2005. Surface and subsurface expressions of gas seepage to the seabed - examples from the Southern North Sea. Marine and Petroleum Geology 22, 499-515.

Shyu, C.T., Hsu, S.K., Liu, C.S., 1998. Heat flows off southwest Taiwan: Measurements over mud diapirs and estimated from bottom simulating reflectors. Terrestrial, Atmospheric and Oceanic Sciences 9 (4), 795-812.

Sloan, E. D., (1990). Clathrate hydrates of natural gases, Marcel Dekker, N.Y., 641.

Tassone, A., Lodolo, E., Menichetti, M., Yagupsky, D., Caffau, M., Vilas, J.F., 2008. Seismostratigraphic and structural setting of the Malvinas Basin and its southern margin (Tierra del Fuego Atlantic offshore). Geologica Acta 6, 55–67.

Thomas, C.R., 1949. Geology and Petroleum Exploration in Magallanes Province, Chile. AAPG Bulletin 33 (9), 1553-1578.

Tissot, B.P., Welte, D.H., 1984. Petroleum Formation and Occurence. Springer-Verlag Berlin Heidelberg New York Tokio, pp. 699.

Uyeda, S., Watanabe, T., Kausel, E., Kubo, M., Yashiro, Y., 1978. Report of Heat Flow Measurements in Chile. Bulletin of the Earthquake Research Institute 53, 131-163.

Weimer, P., 1990. Sequence stratigraphy, facies geometries, and depositional history of the Mississippi fan, Gulf of Mexico. AAPG Bulletin, 74, 425-453.

Wood, W.T., Gettrust, J.F., Chapman, N.R., Spence, G.D., Hyndman, R.D., 2002. Decreased stability of methane hydrates in marine sediments owing to phase-boundary roughness. Nature 420, 656- 660.

Yrigoyen, M.R., 1989. Cuenca de Malvinas. In: Chebli, G., Spalletti, L. (eds). Cuencas Sedimentarias Argentinas. Universidad Nacional de Tucumán, Serie Correlación Geológica 6, 481-491.

Zielinski, G.W., Bruchhausen, P.M., (1983). Shallow temperature and thermal regime in the hydrocarbon province of Tierra del Fuego. AAPG Bulletin 67 (1), 166-177.

990 **Figures:**

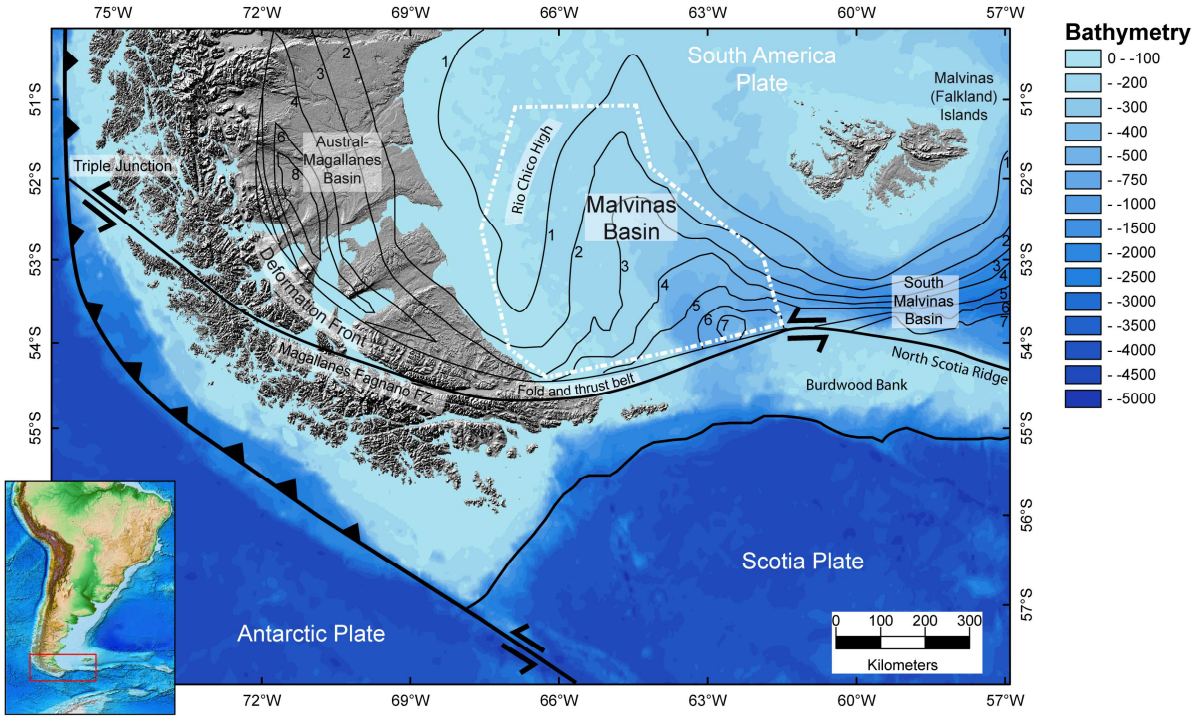

991

992 Figure 1: Tectonic setting of the Malvinas Basin and study area (white dashed line). Contour
993 lines (thin black lines) show the sediment thickness in km deposited in the Malvinas Basin
994 and adjacent areas (modified after Ghiglione et al., 2010). Bathymetry and relief from Amante
995 and Eakins (2009). Read text for detailed description.

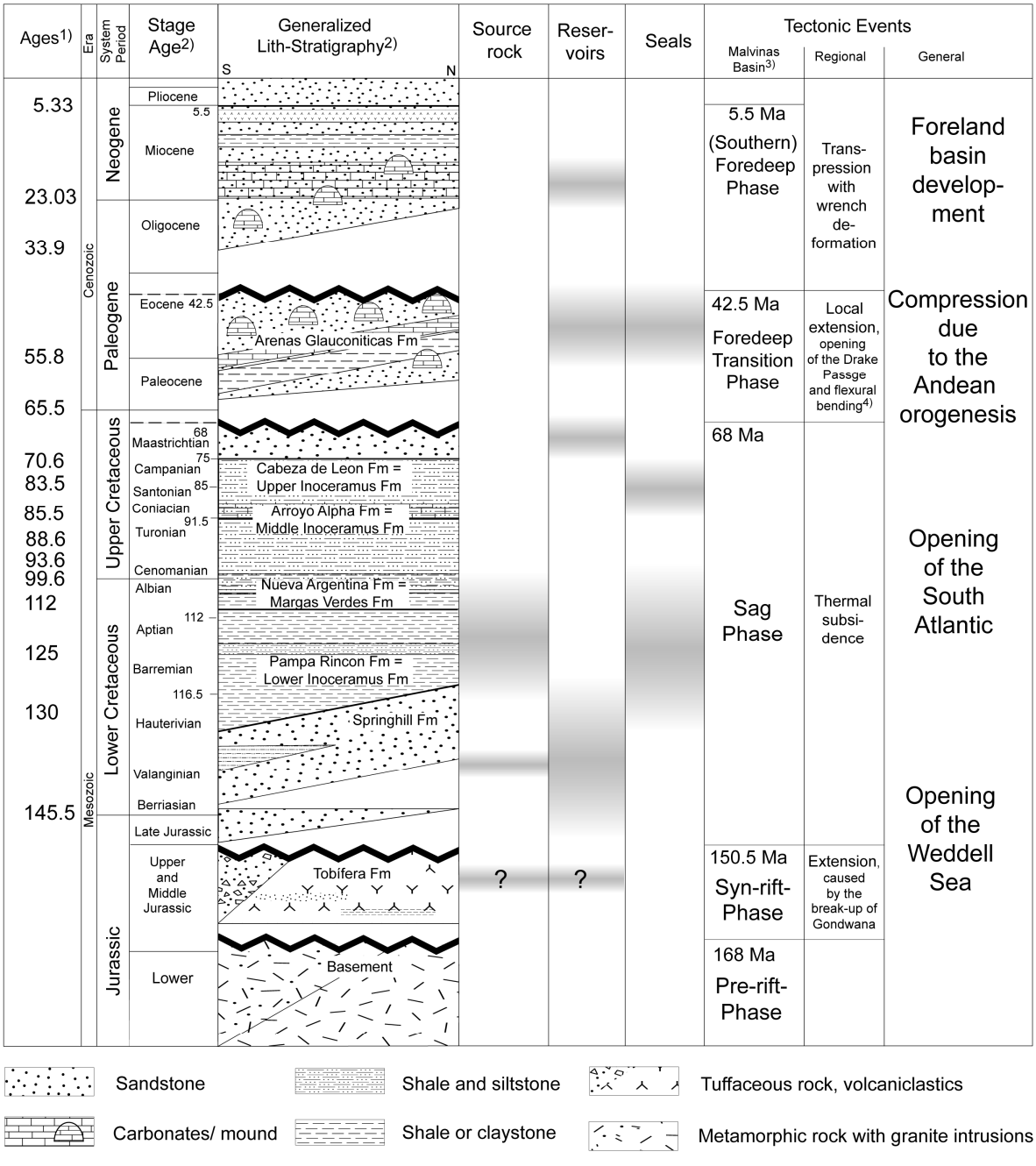

Figure 2: Generalized litho-stratigraphy of the Malvinas Basin with main unconformities, petroleum system elements and main tectonic events (compiled from Biddle et al., 1986; Yrigoyen, 1989; Galeazzi, 1998; Tassone et al., 2008; Ghiglione et al., 2010). 1) ages after Gradstein et al. (2004); 2) modified after Galeazzi (1998) and Yrigoyen (1989); 3) after Galeazzi (1998); 4) Ghiglione et al. (2010).

1003

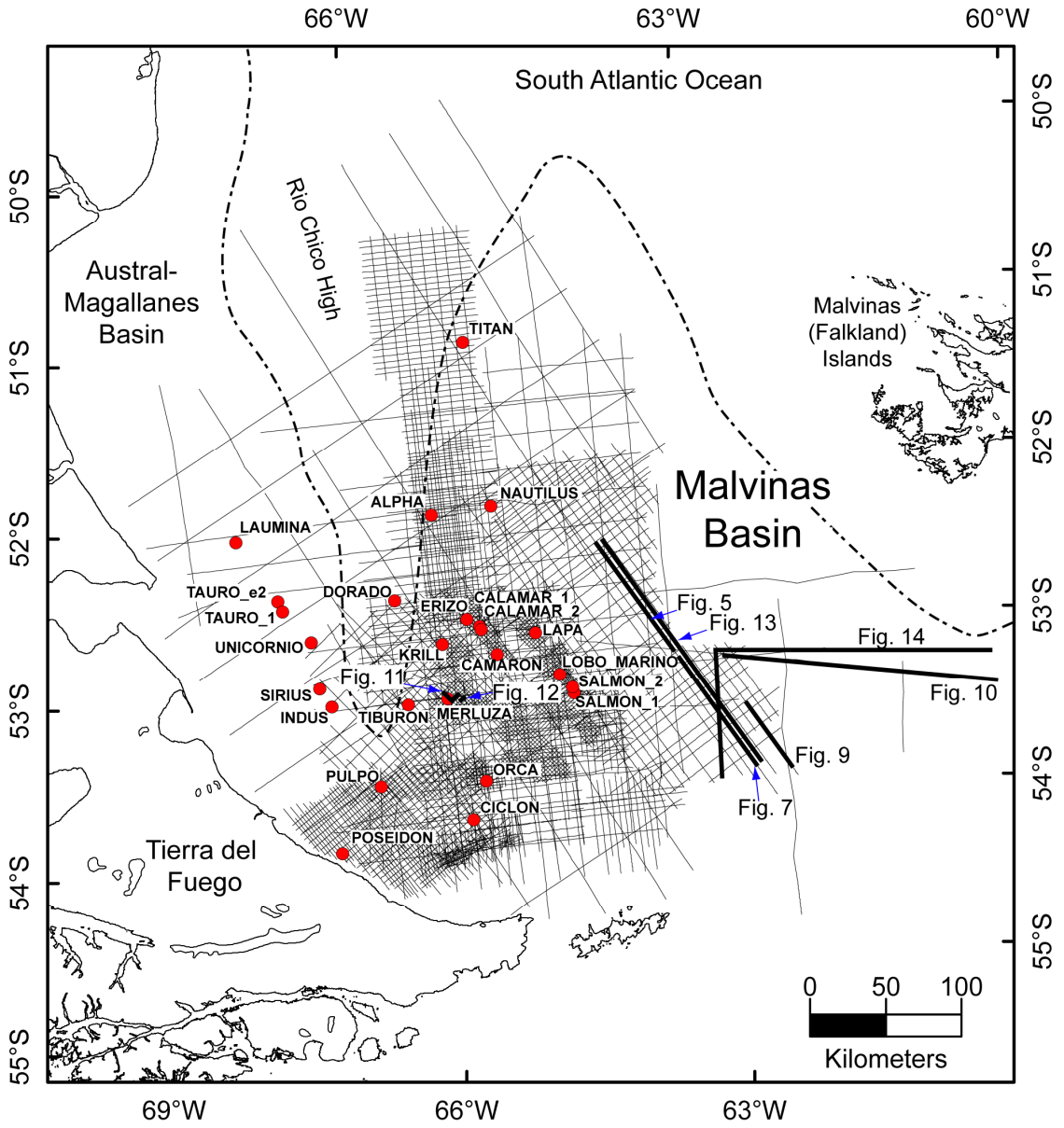

1004
1005 Figure 3: Seismic reflection dataset interpreted in this study (black lines) and well locations

1006 (red dots).

1007

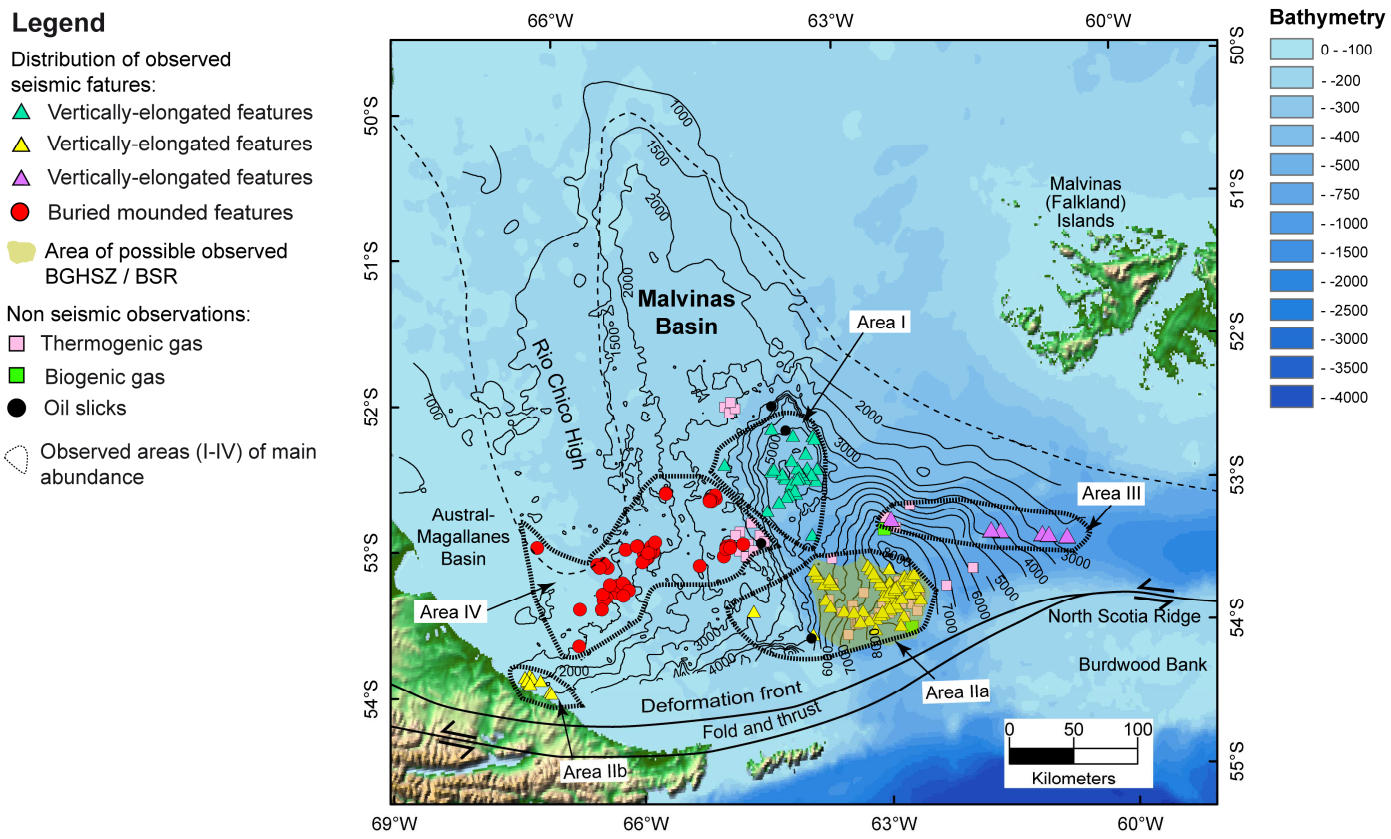

1009

1010 Figure 4: Bathymetric map with defined areas I-IV, the observed most prominent seismic features, area of observed BSR and non seismic leakage

1011 indicators. Basement depth (black lines) in msec (twt) mapped from 2D seismic. Bathymetry and relief from Amante and Eakins (2009).

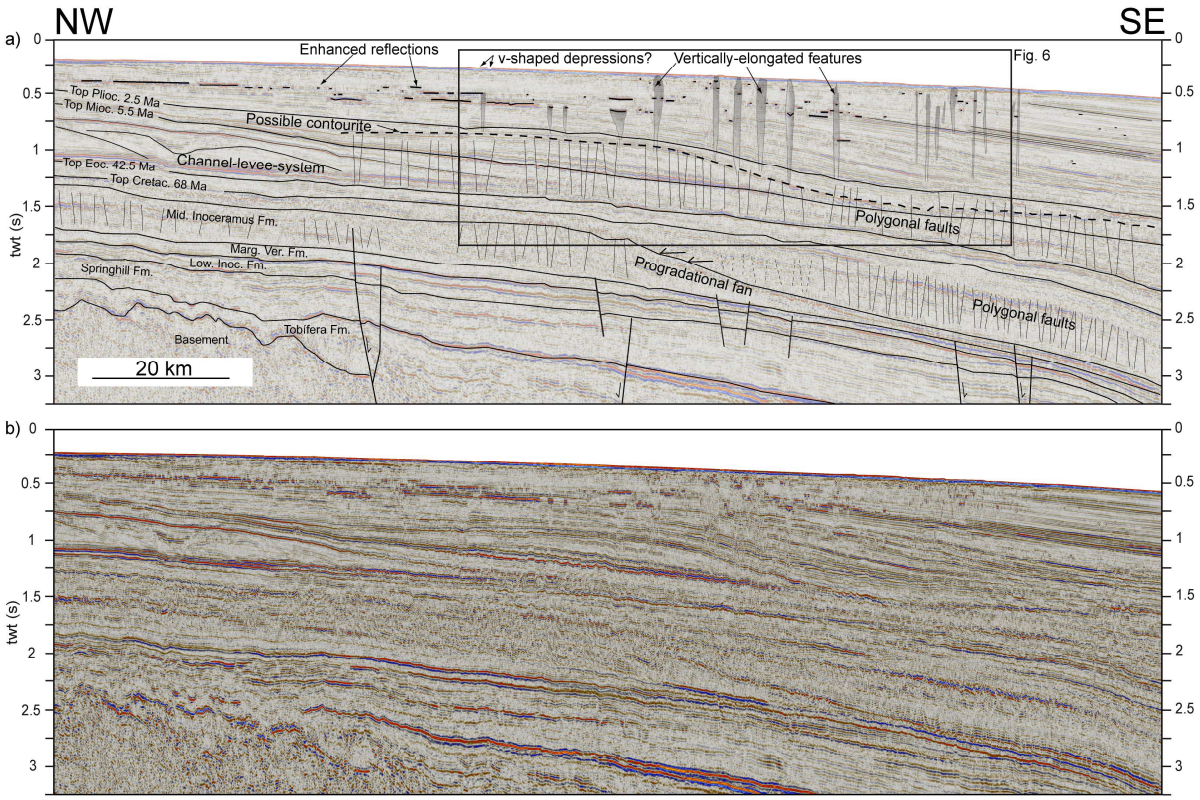

Figure 5: Interpreted (a) and uninterpreted (b) 2D seismic line showing an overview of the observed vertically-elongated features, v-depression on the seabed and enhanced reflections located above polygonal faulted interval. For details shown in the black box see fig 6. (For location see fig. 3).

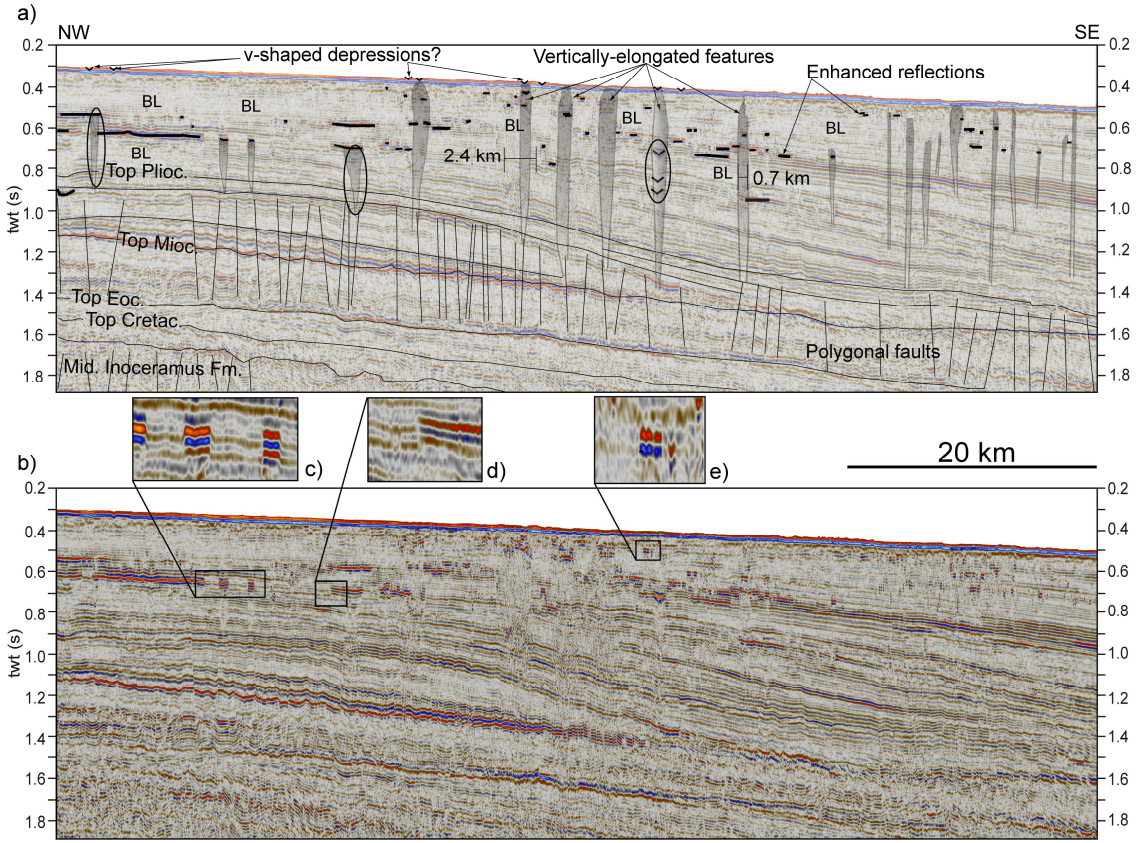

Figure 6: Detail of interpreted (a) and uninterpreted (b) 2D seismic line (Fig. 5) showing vertically-elongated features, v-depression on the seabed and enhanced reflections located above polygonal faulted interval. In the uninterpreted figure b) amplitude inversions are shown within the boxes and the areas with stacked v-shaped depression is indicated within the ellipses in a). (c), (d), and (e) are enlargements of the boxes with an amplitude inversion. BL = blanked area. (For location see figs. 3, and 5).

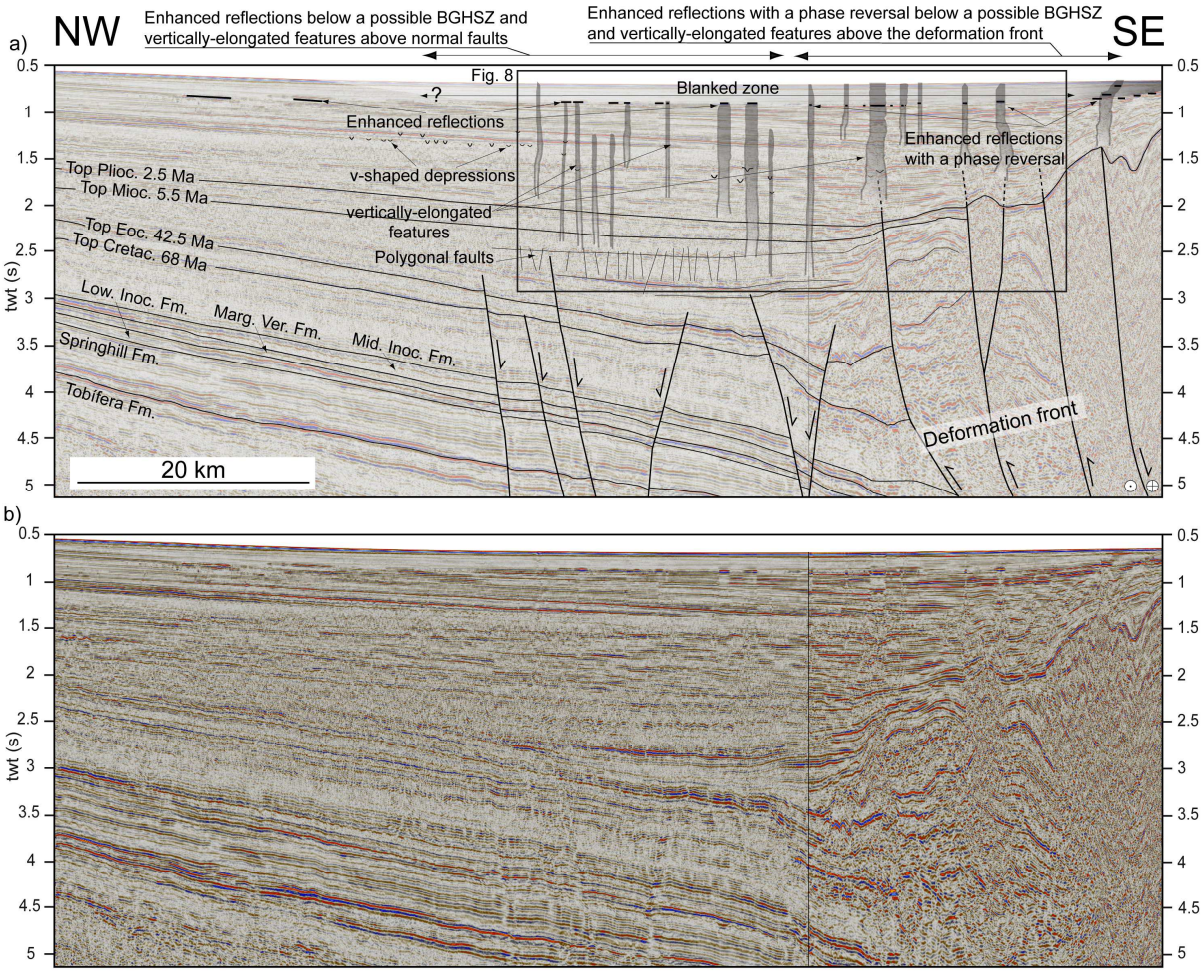

Figure 7: Interpreted (a) and uninterpreted (b) composite 2D seismic line showing examples of vertically-elongated features and leakage indicators in area II in front and above the deformation front. For details shown in the black box see fig 8. (For location see fig. 3).

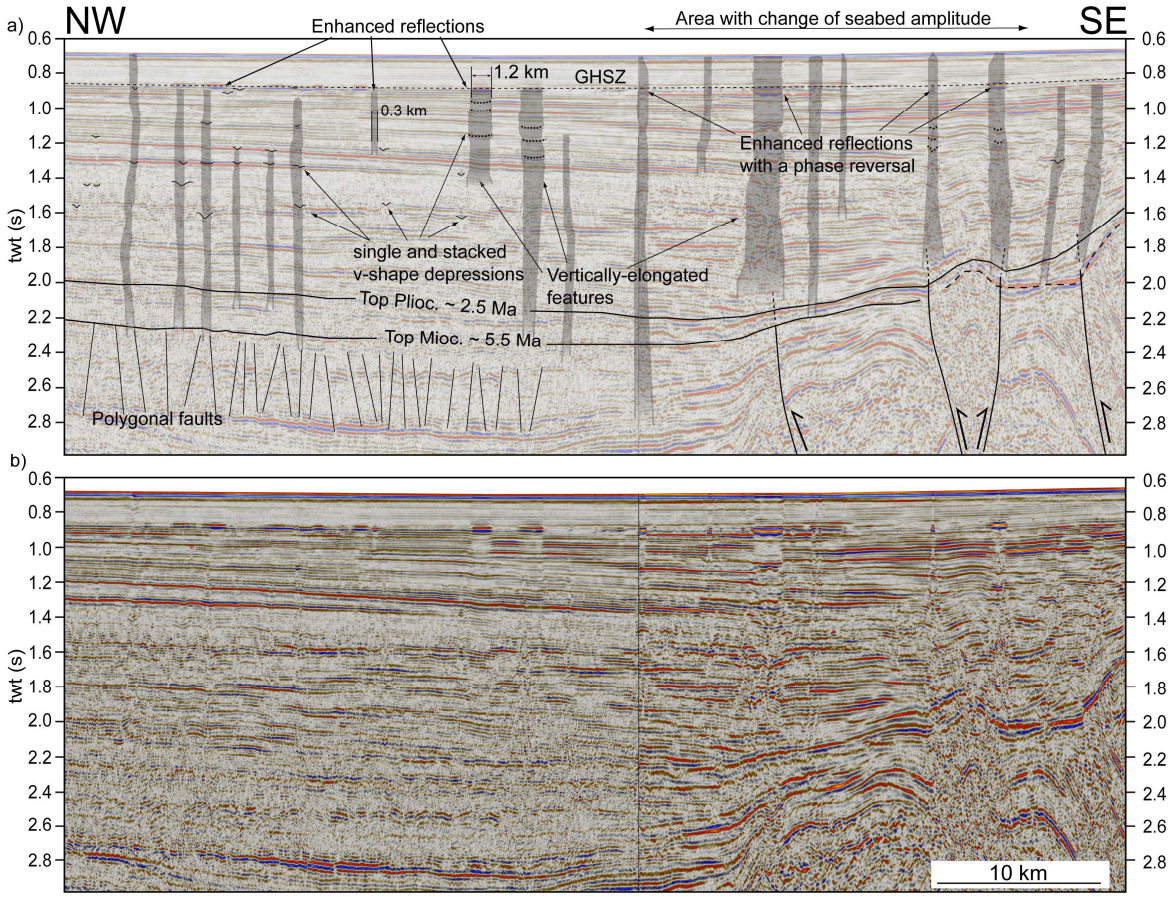

Figure 8: Detail of interpreted (a) and uninterpreted (b) 2D seismic line (Fig. 7) showing vertically-elongated features and leakage indicators in area II above and near the deformation front. Read text for details. (For location see figs. 3, and 7).

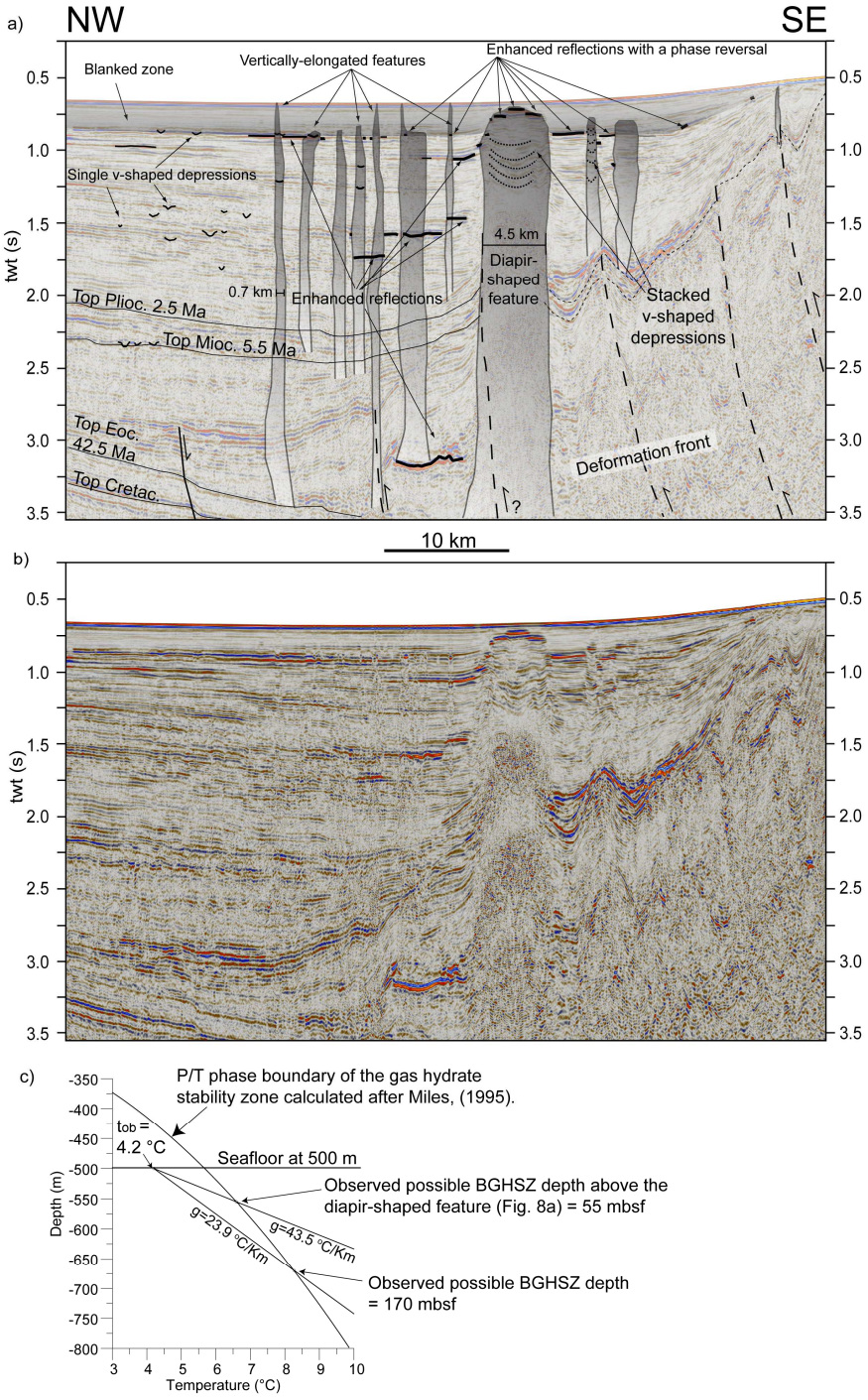

Figure 9: Examples of interpreted (a) and uninterpreted (b) vertically-elongated features in area II, enhanced reflection anomalies with and without a phase reversal, a diapir-shaped vertically-elongated feature, stacked and single v-shaped depressions. (c) is showing the P/T phase diagram of a possible gas hydrate stability boundary calculated after Miles (1995). The calculated geothermal gradient (g) has an error of ± 2.0 °C/km. It corresponds to a possible BGHSZ proposed to be located at the two observed enhanced reflections with a phase reversal

observed in 8a/b and 9a/b above the diaper-shaped feature. t_{ob} = temperature at ocean bottom; mbsf = meter below seafloor. For further information see text. (For location see fig. 3).

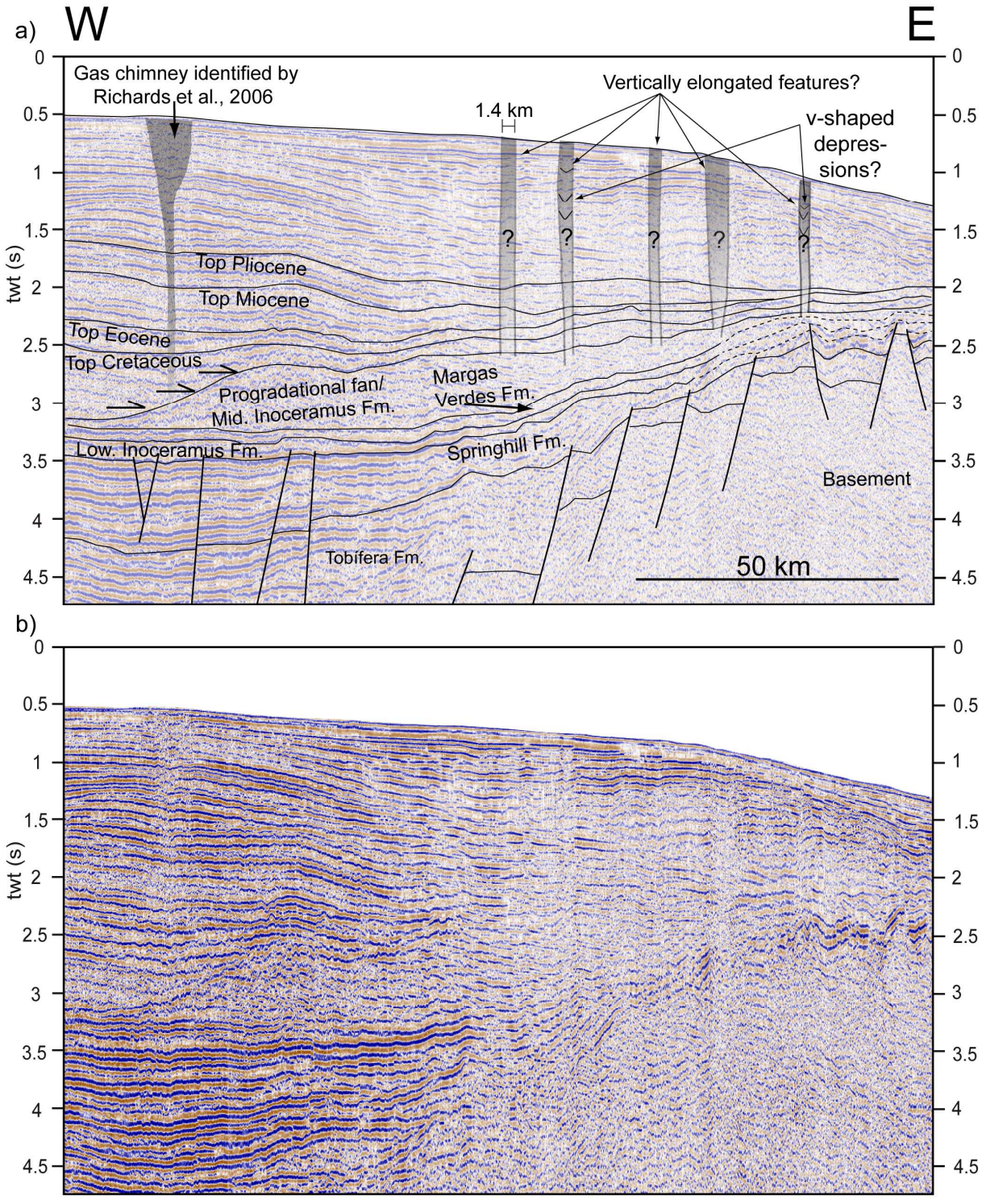

Figure 10: Examples of interpreted (a) and uninterpreted (b) vertically-elongated features in area III. (For location see fig. 3).

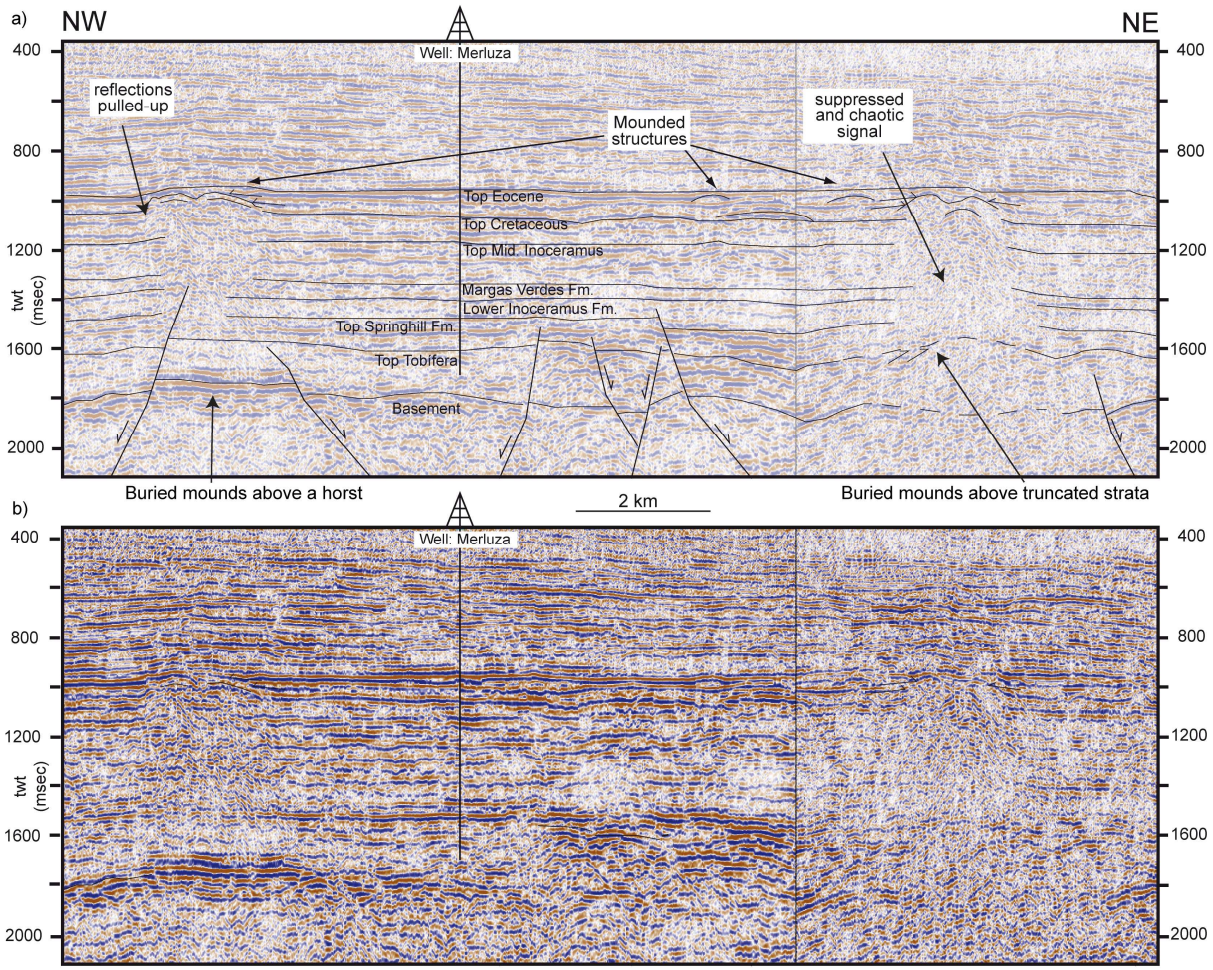

1044

1045

1046 Figure 11: Composite seismic 2D line showing interpreted (a) and uninterpreted (b) Eocene

1047 buried mounded structures. (For location see fig. 3).

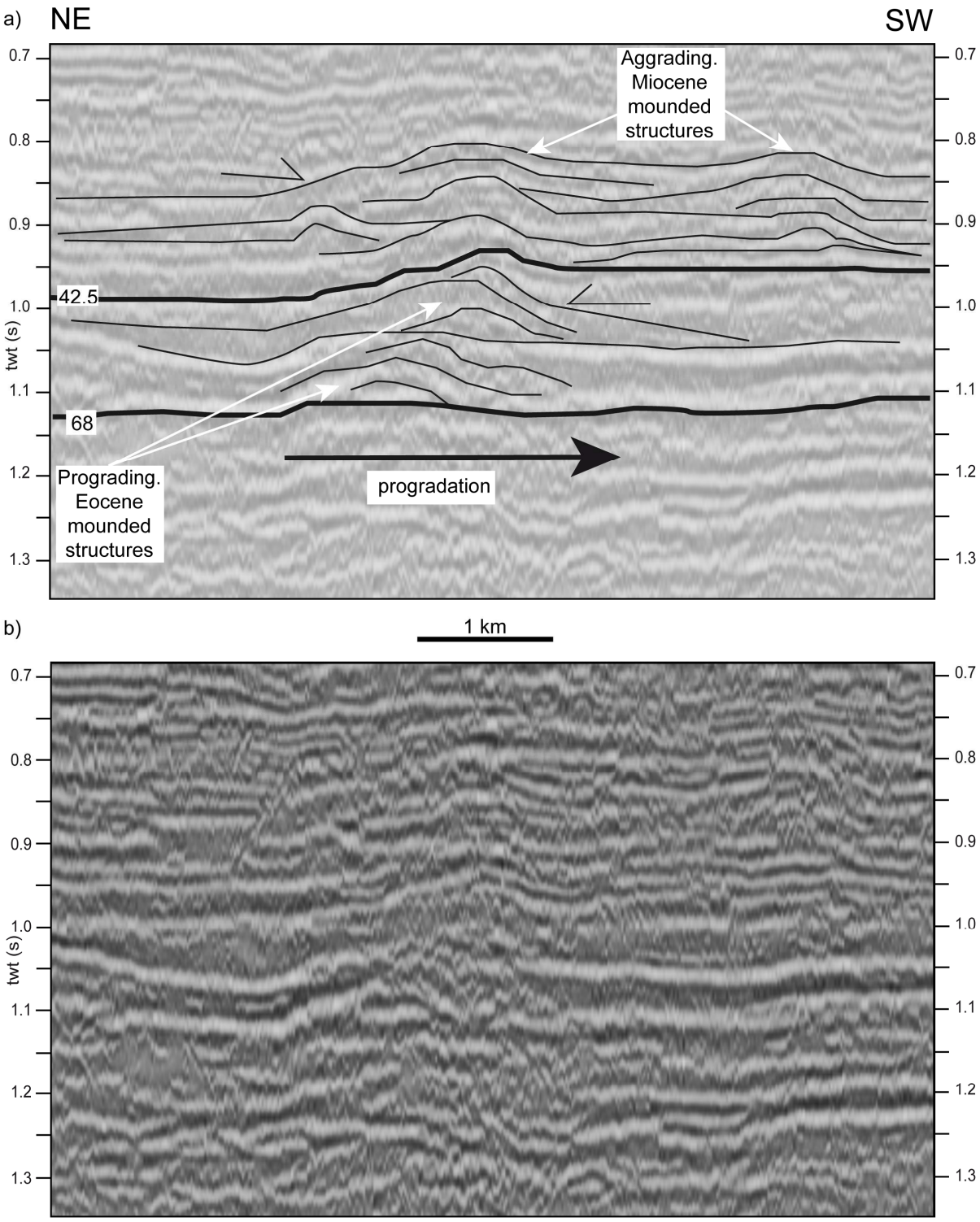

1048

1049

1050 Figure 12: Examples of interpreted (a) and uninterpreted (b) asymmetric and symmetric

1051 buried Eocene and Miocene mounded structures with internal progradation pattern during

1052 Eocene and internal aggradation pattern during Miocene. Thick black lines represent ages in

1053 Ma of the main unconformities. (For location see fig. 3).

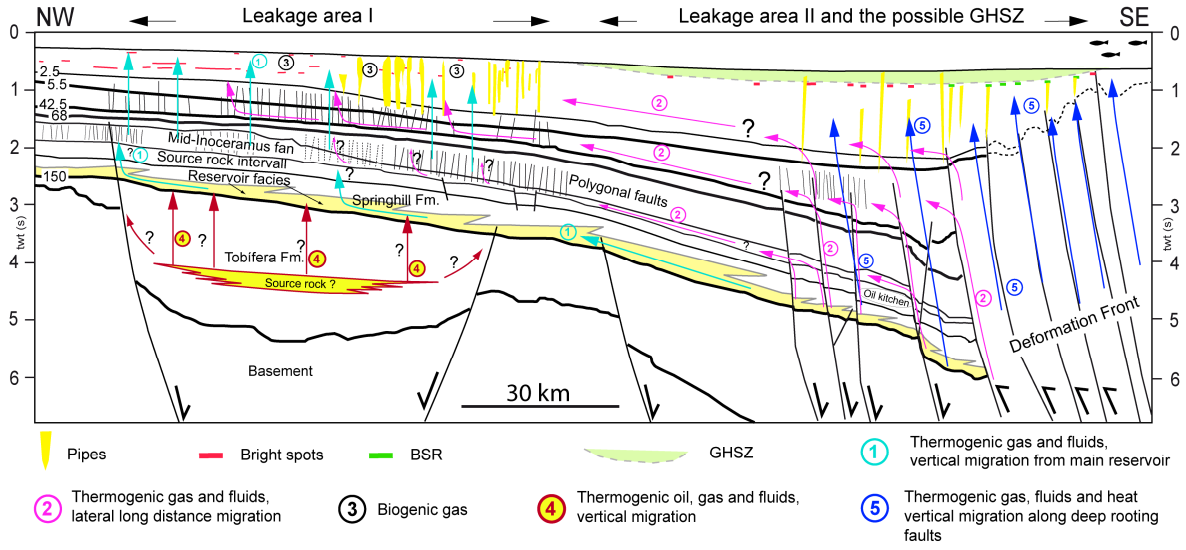

1054

1055

1056 Figure 13: Sketch of composite seismic lines of figs. 5, and 7 and proposed possible leakage

1057 pathways responsible for active leakage populations in area I and II. Age of main

1058 unconformities in Ma. (For location see fig. 3).

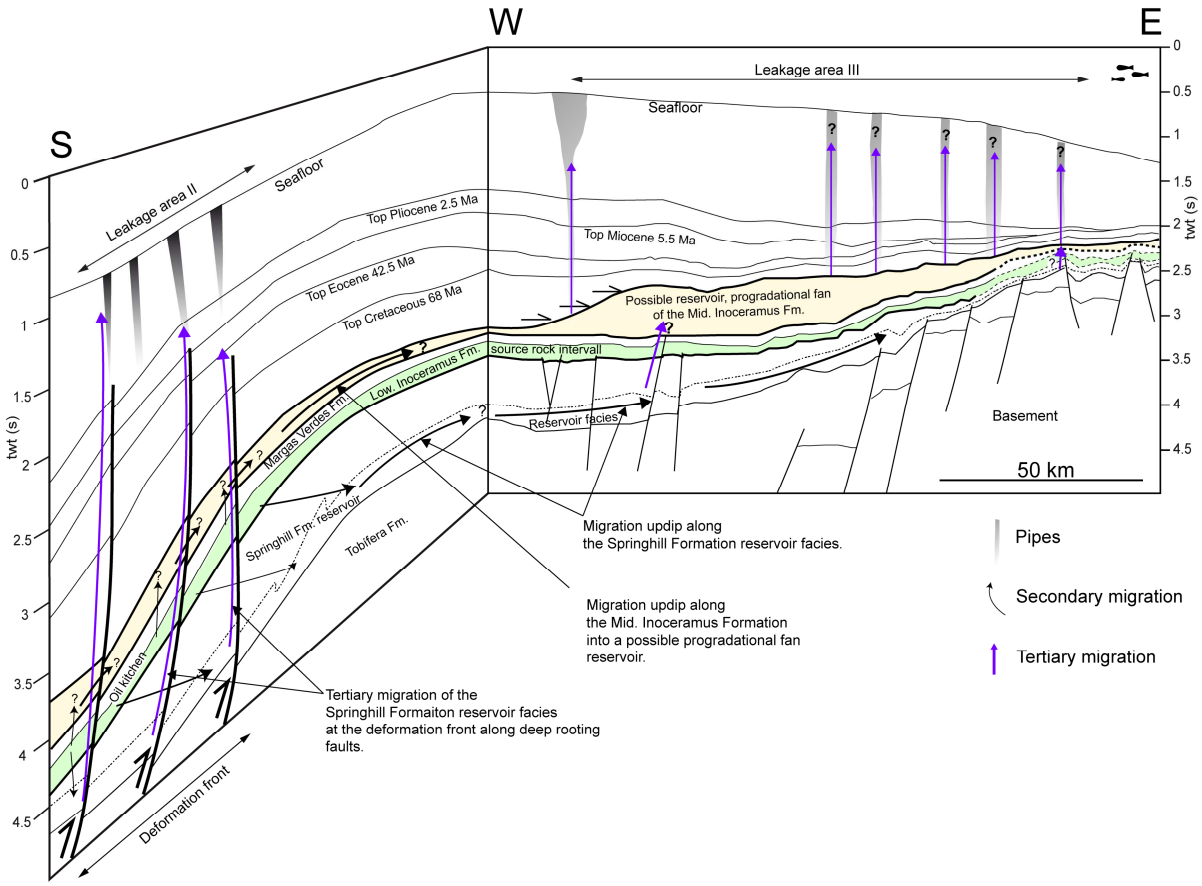

Figure 14: Sketch of composite seismic lines of figs. 7 and 10 and proposed possible leakage pathways responsible for active leakage populations in area II and III. (For location see fig. 3).